Visible Light Induced Photocatalytic Performance of Mn-Sno2@Zno Nanocomposite for High Efficient Cationic Dye Degradation

S. Asaithambi
Alagappa University
P. Sakthivel
Alagappa University
M. Karuppaiah
Alagappa University
V. Balaji
Alagappa University
R. Yuvakkumar
Alagappa University
Ravi G (gravicrc@gmail.com)
Alagappa University https://orcid.org/0000-0003-4493-1539

Research Article

Keywords: Mn-SnO2@ZnO heterojunction, Methylene blue and Rhodamine B

Posted Date: March 10th, 2021

DOI: https://doi.org/10.21203/rs.3.rs-298961/v1

Version of Record: A version of this preprint was published at Journal of Materials Science: Materials in Electronics on August 3rd, 2021. See the published version at https://doi.org/10.1007/s10854-021-06692-x.

VISIBLE LIGHT INDUCED PHOTOCATALYTIC PERFORMANCE OF Mn-SnO_2@ZnO NANOCOMPOSITE FOR HIGH EFFICIENT CATIONIC DYE DEGRADATION

S. Asaithambi[1,2], P. Sakthivel[1], M. Karuppaiah[1], V. Balaji[1], R.Yuvakkumar[1], G. Ravi[1]*

[1]Department of Physics, Alagappa University, Karaikudi-630003, Tamil Nadu, India.

[2]Department of Engineering and Science, Western Norway University of Applied Sciences, Bergen, 5063, Norway

*Corresponding author: *gravicrc@gmail.com*.Telephone: +914565-225206.

Abstract

In this work, we have synthesized Mn-doped SnO_2@ZnO nanocomposite for photo degradation of Methylene blue and Rhodamine B dyes upon visible light irradiation. The crystal structure, functional group, optical absorption, defect related emission, morphology, purity and binding energy state of synthesized samples were identified by using various analytical tools. The optical absorption shift and the reduction of band gap values are confirming the formation of hetero-junction of SnO_2@ZnO composites. The Mn-SnO_2@ZnO hetero-junction effectively induces the photo-generated charge carrier separation and enriches the charge transfer which helps in enhancing the photo-catalytic activities. The photocatalytic degradation results clearly indicate that the Mn-doped SnO_2@ZnO nanocomposite has higher degradation efficiency of 98 % and 92 % for the Methylene blue and Rhodamine B dyes, respectively and is higher than the other synthesized samples. The present study reveals a low cost and highly efficient photo-catalyst which works up on visible light irradiation for the purification of waste water from industries.

Key words: Mn-SnO_2@ZnO heterojunction, Methylene blue and Rhodamine B

1. Introduction

In the present digital era, the energy shortage and the environmental related problems are the two main issues of the livegoods of the modern society. Each year, the Sun releases 1.5×10^{18} kW h energy to earth which is nearly equal to 28,000 times of the energy consumption

per year. There are various techniques employed for solar energy utilization indirectly. Among them, photocatalysis is one of the green techniques used to remove the hazardous organic compounds by solar or visible light irradiation. The photocatalysis is modernized after innovating water photolysis of TiO_2 in 1972 by Fujishima and Honda [1-3]. Currently, the researchers have focused on developing the low cost, low maintenance and high efficient photocatalysts which work upon solar or visible light irradiation to give pollution free water. In the past three decades, the inorganic metal-oxide (TiO_2, SnO_2, CuO, WO_3 and ZnO, etc) based semiconducting materials have propelled a great attention in the field of photocatalysis due to their high catalytic behavior and stability [4-7]. Among the metal oxides, SnO_2 is an excellent photocatalyst because it has good transparency, high photosensivity, good stability, and also it is low cost and eco friendly. Several strategies have been employed to reduce the band gap and enhance the visible light absorption like adding impurity ions, surface sensitization and formation of heterojunction with semiconductors [8-9]. Recently, doping impurity ions like Cu, Co, Ni, Mn and Fe with SnO_2 has been found to enhance the photocatalytic activities considerably [10-14]. However, the dopant ions could not enhance the photocatalytic activity considerably in the visible light region. In this regard, the metal doped SnO_2 added with another metal oxide to form heterojunction may help to further reduce the band gap energy and recombination of electron hole pairs and enrich the visible light absorption [15].

In recent days, semiconductor hetero-junction was formed to promote the visible light induced photocatalytic application. H. Xia *et.al,* reported Fe_2O_3/SnO_2 based photocatalyst using acid blue 62 dye which underwent a maximum of 98% degradation [16]. X. Hui-li *et. al,* synthesized CuO-SnO_2 nanocomposite using acid blue 62 dye under visible light irradiation [17]. S.H. Hwang *et.al,* prepared SnO_2-TiO_2 nano-fiber catalyst for photo-degradation of Rhodamine B [18]. B.C. Zhu *et.al,* prepared SnO_2/Fe_2O_3 heterojunction nanotubes for visible light photocatalytic degradation [19]. H.R. Pouretedal *et.al,* have reported about a mixture of ZrO_2/SnO_2 for degradation of 2-nitrophenol [20]. A. Priyadharsan *et.al,* prepared ternary CeO_2/SnO_2/rGO composite for degradation of methylene blue dye using visible light [21]. M.A. Subhan *et.al,* reported NiO·CeO_2·ZnO based composite which revealed the high efficiency photocatalytic application [22]. Karuthapandian *et.al,* prepared CuO–ZnO nanorods and the photocatalytic performance was measured for Congo red and Rhodamine B [23]. J. Lin et al prepared ZnO/SnO_2 photocatalyst and it offered 98% MB degradation [24]. Among them, SnO_2-

ZnO based heterostructure photocatalyst has received a great attention, because ZnO is an *n*-type semiconductor, non-toxic, low cost, has good photosensitivity, and high photo-stability with a high exciton binding energy (60 meV) [25]. The SnO_2-ZnO based heterostructure has good band position which reduces the recombination of charge carrier, stimulate the charge separation and enrich the photocatalytic activity. Earlier, so many researchers reported the SnO_2 and ZnO based composites for visible light based photocatalytic application. However, the metal doped SnO_2@ZnO based composites have rarely reported. Recently, the doping of transition metal has great attention in the field of photocatalytic application, because transition metals reduce the particle size, increase the surface area, stimulate the absorption in the visible region and reduce the recombination of electron-hole pairs. Among the transition metals, Mn is superior because it has different valence states (Mn^{2+}, Mn^{3+} and Mn^{4+}) which easily replace the Sn^{4+} ions of the SnO_2 lattice. The Mn ions also produce the above mentioned effects which helped to enrich the photocatalytic activity [26, 27].

In this work, we have synthesized Mn-doped SnO_2@ZnO nanocomposites for photocatalytic degradation of cathodic dye under visible light irradiation. For the synthesized samples, structural, optical, composition and morphology were analyzed by using various analytical tools. When compared to SnO_2, Mn-SnO_2, SnO_2@ZnO samples, the Mn-SnO_2@ZnO composite exhibit a maximum degradation efficiency of 98 % and 92% for Methylene blue and Rhodamine B dyes under visible light irradiation.

Experimental Techniques

Materials Used

Tin-chloride-dihydrate ($SnCl_2.2H_2O$), zinc-chloride ($ZnCl_2$), manganese-chloride tetrahydrate ($MnCl_2.4H_2O$), sodium hydroxide (NaOH) and ammonium hydroxide (NH_4OH) chemical reagents were used in this work. All the chemicals with purity of 99.99 % were purchased from Sigma Aldrich and used without any further purification.

Synthesize of ZnO nanoparticles

Initially, 0.1 M $ZnCl_2$ was added with 100 ml doubly distilled water and 0.4 M NaOH solution was added drop wise until the pH of the solution reach 9. Then, the hydroxide solution

was stirred for 30 min at room temperature. Thereafter, the obtained white precipitate was washed with water and ethanol to remove impurities. Then, the precipitate was dried at 100 ºĊ for 12 h and the resultant powder was annealed at 300 ºĊ for 4 h.

Synthesize of SnO_2, Mn-SnO_2, SnO_2@ZnO and Mn-SnO_2@ZnO composites

Firstly, 0.1 M $SnCl_2.2H_2O$ was dissolved in 100 ml water and the solution was continuously stirred for 30 min. Then, the pH was adjusted to 9 by adding NH_3OH solution drop wise and then the solution was changed to milky white color. Further, the formed tin-hydroxide precipitate was continuously stirred for 3 h to get homogeneous mixing of the precipitate in the solution and then it was washed with water and ethanol. Finally, the precipitate was dried at 100° C for 12 h and annealed at 600° C for 5 h. The same method was followed to synthesize (Mn-5 mM) Mn-SnO_2 nanoparticles. The SnO_2@ZnO and Mn-SnO_2@ZnO composites were synthesized by taking $SnCl_2.2H_2O$ and $ZnCl_2$ in the ratio of 0.06:0.04 M respectively.

Photocatalytic analysis

Photocatalytic performance of the SnO_2, Mn-SnO_2, ZnO, SnO_2@ZnO and Mn-SnO_2@ZnO samples was analyzed by using cationic Metheylene blue (MB) and Rhodamine B (RhB) dyes under the visible light irradiation. Firstly, 100 mg of prepared catalyst and 1 ml MB dye solution were blended with water (99 ml). Then, this solution was sonicated for 10 min to attain homogeneous mixing of dye solution and the synthesized photo-catalyst. Further, the homogeneously mixed solution was kept in a dark environment to get adsorption-desorption equilibrium level. In this work, all the photocatalytic experiments were carried out under the irradiation using a halogen lamp. At a regular interval of 20 min time, 3 ml of reacted suspension was taken to analyze the degradation performance of the solution. The maximum absorbance peak was appeared at ~ 660 nm and ~550 nm for MB and RhB dyes respectively and the absorbance was measured with the help of UV–Vis spectroscopy.

Experimental details

Different analytical techniques have been used to analyze the crystal structure, functional groups, morphology, optical properties, binding energy of the synthesized SnO_2, Mn-SnO_2, ZnO, SnO_2@ZnO and Mn-SnO_2@ZnO composites respectively. The PANalytical X'Pert pro X-ray

diffractometer (λ = 1.5418 Å) and the FTIR spectrometer (Thermo Nicolet 380) were used to identify the crystal structure and functional groups of the synthesized samples. The optical properties were recorded using UV-Vis spectrometer (Thermo Fisher Evolution 220) and photoluminescence spectrometer (Cary Eclipse PL spectrograph) respectively. The surface morphology of the synthesized samples was studied using a field emission scanning electron microscope (FEIQUANDA 200F FESEM). The X-ray Photoelectron Spectroscopy ((Omicron nanotechnology (Oxford instrument)) was used to determine the composition, binding energy and oxidation states of the elements present in the synthesized SnO_2@ZnO and Mn-SnO_2@ZnO composite samples.

Results and Discussion

Powder X-ray diffraction analysis

The crystal structure of the synthesized SnO_2, Mn-SnO_2, ZnO, SnO_2@ZnO and Mn-SnO_2@ZnO composite samples were analyzed using powder X-ray diffraction (PXRD) data. Figure 1 shows the PXRD of synthesized SnO_2 and Mn-SnO_2 nanoparticles which revealed the rutile, tetragonal crystal structure with the space group of *P4₂/mnm* and it is well matched with JCPDS card. No: 41-1445. The pure ZnO exhibited the hexagonal wurtzite structure of ZnO (JCPDS card no. 36-1451) with a crystal space group of *P63mc*. The SnO_2@ZnO and Mn-SnO_2@ZnO composite samples revealed the major intensity peaks of both SnO_2 and ZnO and are depicted in the figure 1.When compared to SnO_2, Mn-SnO_2 and ZnO samples, the Mn-SnO_2@ZnO has lower intensity peaks which may be due to the doping of Mn in SnO_2 sites and the addition of ZnO. The Debye-Scherer formula has been used to determine the average crystallite size of the synthesized samples and the relation is as follows [28, 29]

$$D = \frac{0.94\times\lambda}{\beta cos\theta}\,(\text{nm}) \qquad (1)$$

where, D is crystallite size (nm), λ is X-ray wavelength (nm), β is full width half maximum of diffraction peak (rad), and θ is diffraction angle (degree). The average crystallite size was found to be 23.3nm, 21.6 nm, 27.7nm, 20.6 nm and 16.7 nm for the SnO_2, Mn-SnO_2, ZnO, SnO_2@ZnO and Mn-SnO_2@ZnO composite samples; the Mn-SnO_2@ZnO composite was found to having relatively smaller crystallites when compared to the other samples. The Mn and Zn ions

minimize the growth rate and nucleation of the SnO_2 structure. The lower crystallite size helps in increasing the surface area and it may also enhance the photocatalytic activities.

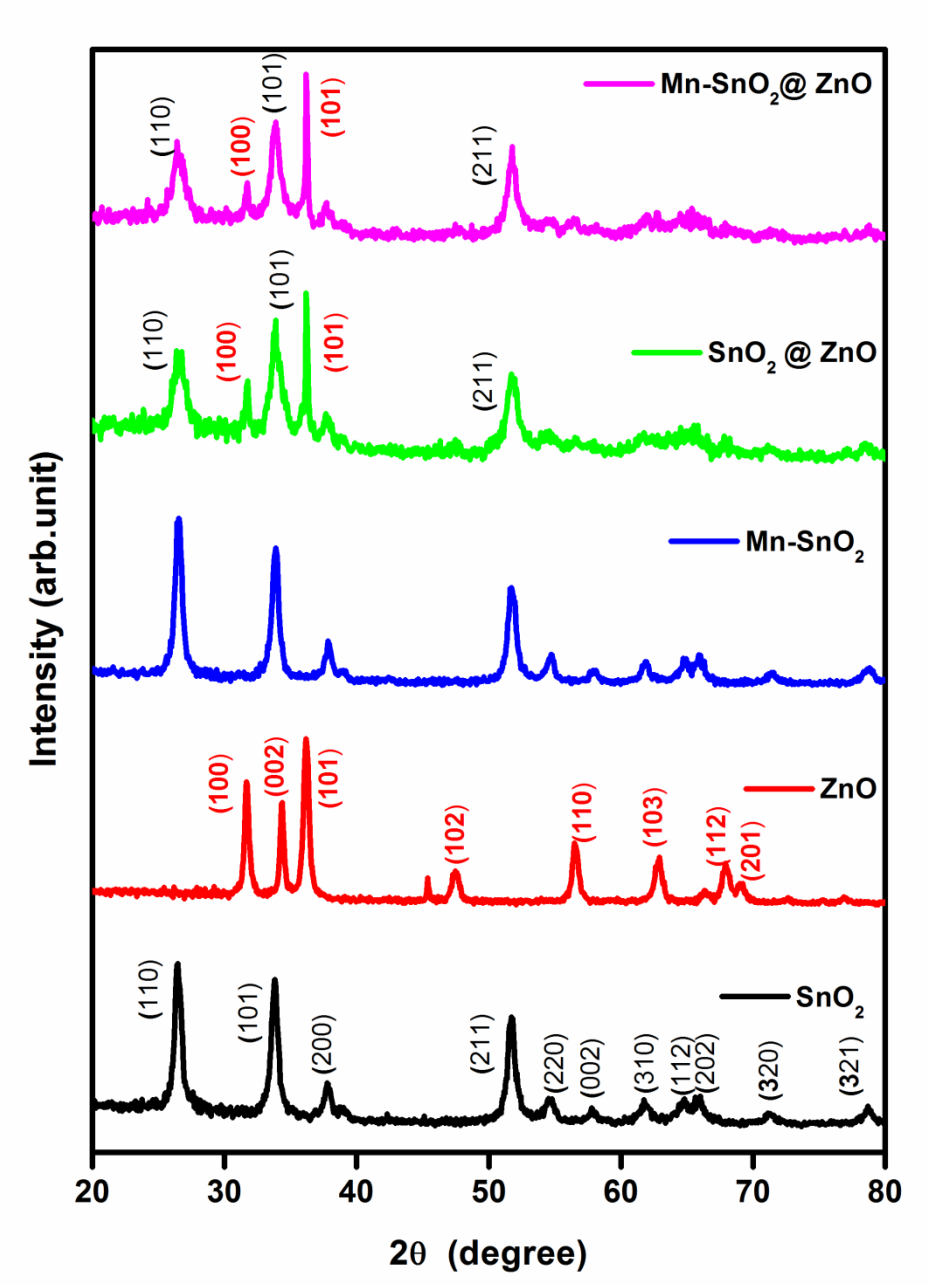

Figure 1 PXRD pattern of synthesized SnO_2, ZnO, Mn-SnO_2, SnO_2@ZnO and Mn-SnO_2@ZnO composite samples.

Fourier transform infrared spectroscopy analysis

Figure 2 depicts the Fourier transform infrared (FTIR) spectra of the synthesized SnO_2, Mn-SnO_2, ZnO, SnO_2@ZnO and Mn-SnO_2@ZnO composite samples. A strong peak appeared at 665 cm^{-1} and 558 cm^{-1} correspond to the Sn–O–Sn and Sn–O stretching vibrations, respectively, and it confirms the formation of rutile, tetragonal structure of the SnO_2 and Mn-SnO_2 samples. A small ZnO vibration peak observed at 461 cm^{-1} is related to Zn–O stretching mode. In the SnO_2@ZnO and Mn-SnO_2@ZnO composite samples, the FTIR spectra revealed both Sn–O–Sn stretching and Zn–O stretching modes around 620 cm^{-1} and 488 cm^{-1} respectively [30,31]. In addition, the OH stretching and bending vibration modes observed around ~3430 cm^{-1} and ~1620 cm^{-1} which are due to the absorption of water molecules on the surface of the synthesized samples. The small absorption changes were observed in the composite samples due to the addition of Mn and Zn in SnO_2 sites. The FTIR spectra also confirm the presence of ZnO and SnO_2 elements which is in good agreement with the PXRD results.

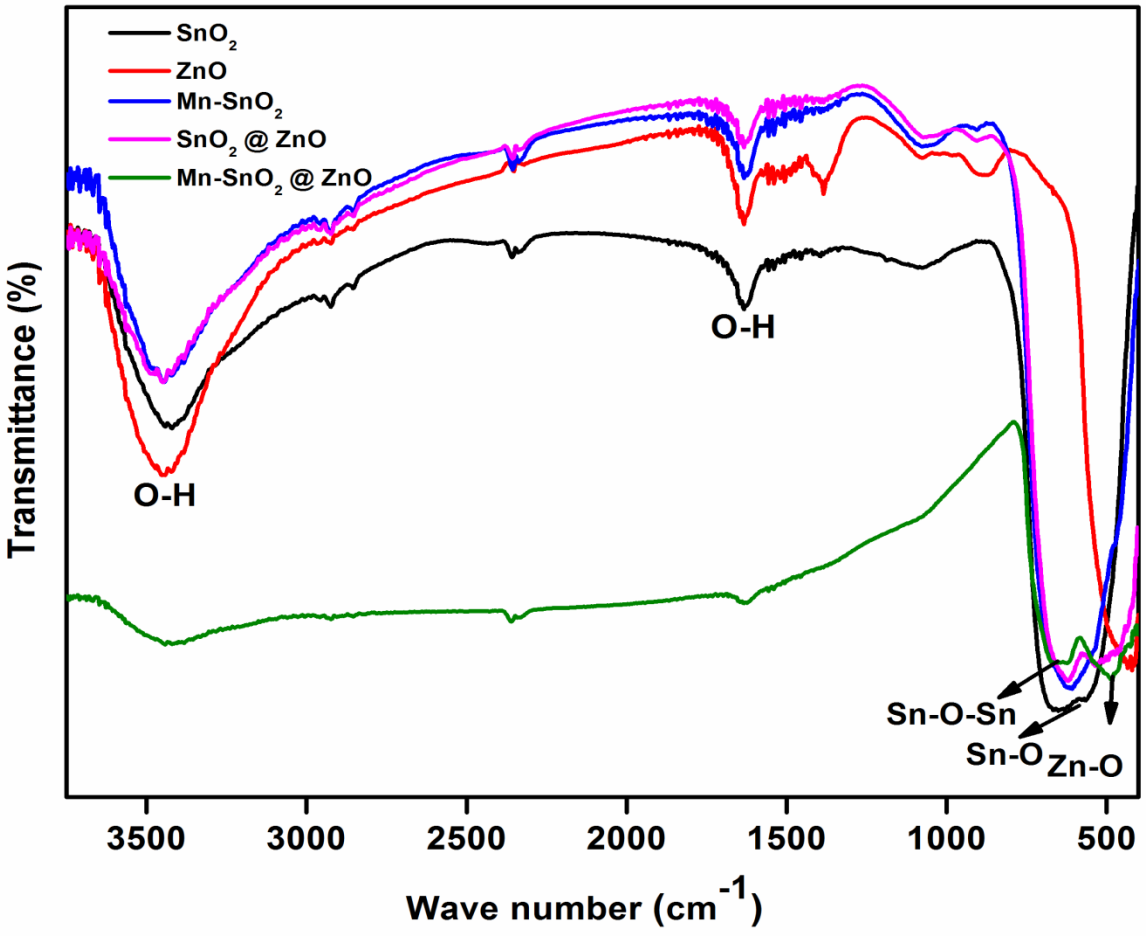

Figure 2 FTIR spectra of the synthesized SnO_2, Mn-SnO_2, ZnO, SnO_2@ZnO and Mn-SnO_2@ZnO composites samples.

UV-visible spectra analysis

UV-Visible absorption properties of the synthesized SnO_2, Mn-SnO_2, ZnO, SnO_2@ZnO and Mn-SnO_2@ZnO composite samples were analyzed in the range of 200-800 nm at room temperature and the absorption spectra are shown in figure 3 (A). The maximum absorption peaks were observed at 278 nm, 288 nm and 358 nm for the SnO_2, Mn-SnO_2 and ZnO nanoparticles. Further, the maximum absorption peaks were slightly shifted in the higher wave length side (red shift) due to the formation of SnO_2@ZnO heterostructures and also the maximum absorption peak of SnO_2@ZnO and Mn-SnO_2@ZnO composite samples were appeared in between the absorption peaks corresponding to SnO_2 and ZnO. The absorption edges were found in between 390-460 nm for all the synthesized samples. In addition, the band gap energies of all the synthesized samples were estimated by using Tauc plots using the relation given below [11, 32]:

$$\alpha h\nu = A\left(h\nu - E_g\right)^n$$

where, α is the absorption coefficient, ν is the frequency, h is the Plank's constant, A is a constant, E_g is the Energy gap and $n = ½$ for the direct band gap of the semiconductors.

The estimated energy band gap values are 3.52, 3.32, 3.01, 3.12 and 2.77 eV for the synthesized SnO_2, Mn-SnO_2, ZnO, SnO_2@ZnO and Mn-SnO_2@ZnO composite samples, respectively and are shown in figure 3 (B). The Mn-SnO_2@ZnO composite has a lower band gap values compared to all other synthesized samples, which may be due to the addition of Mn in SnO_2 sites and Zn ions respectively. When adding the metals in SnO_2, the peak position was moved to higher wavelength sides and it would help to enhance the strength of visible light absorption. The UV-visible spectra revealed the visible light absorption by the composite samples which induce enhanced photocatalytic efficiency of the composite samples.

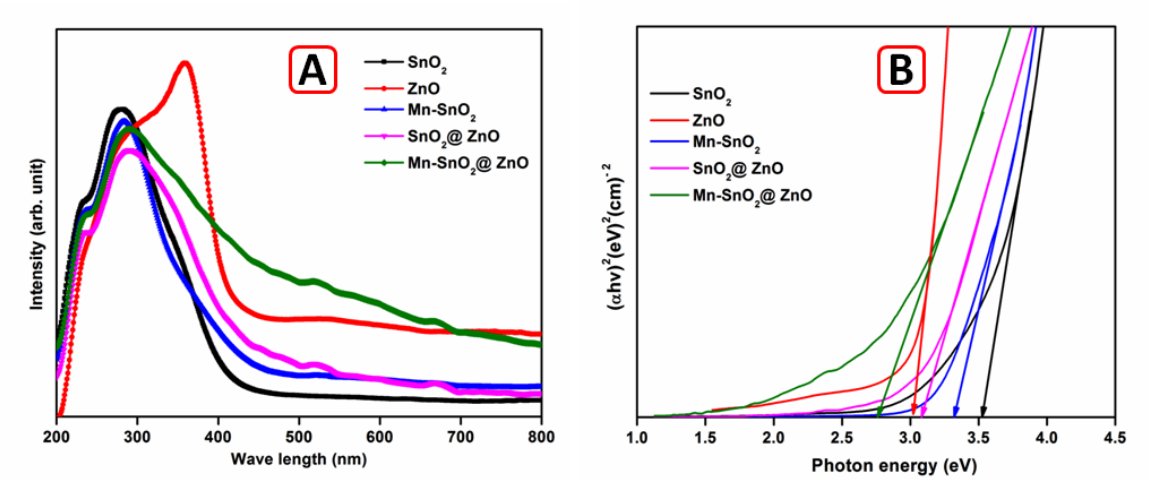

Figure 3 (A) UV-visible absorption spectra, (B) Tauc plots of synthesized SnO_2, Mn-SnO_2, ZnO, SnO_2@ZnO and Mn-SnO_2@ZnO composite samples.

Photoluminescence Analysis

The photoluminescence (PL) is one of the versatile techniques used to determine the surface defects and oxygen vacancies of the prepared samples. Figure 4, depicts the photoluminescence spectra of the synthesized SnO_2, Mn-SnO_2, ZnO, SnO_2@ZnO and Mn-SnO_2@ZnO composite samples and it was recorded using an excitation wavelength of 320 nm. The pure SnO_2 spectra revealed five emission peaks that are centered at 361 nm, 377 nm, 411 nm, 437 nm and 489 nm respectively. In the UV region, the near band edge (NBE) emission peak observed at 361 nm and 377 nm. The blue-violet and blue emission related peaks are observed at 411 nm and 437 nm and are due to the electron recombination with shallow level defects and surface defects of the SnO_2 nanoparticles [12]. The pure ZnO shows four different emission peaks: (1) a sharp UV band emission peak centered at 390 nm which is related to the near band edge emission, (2) a violet band was observed at 409 nm, (3) a low intensity peak appeared at 438 nm corresponds to a blue band, (4) a sharp bluish-green emission peak centered at 490 nm respectively [33]. When compared to pure and doped samples, the SnO_2@ZnO and

Mn-SnO_2@ZnO composite samples have higher intensity peaks which are due to the incorporation of Mn in the SnO_2 sites and the addition Zn ions. This creates more oxygen vacancies and surface defects in the synthesized samples. The surface defects and the oxygen vacancies enhance the photocatalytic activities and the Mn-SnO_2@ZnO composite has a higher photocatalytic efficiency when compared with other samples.

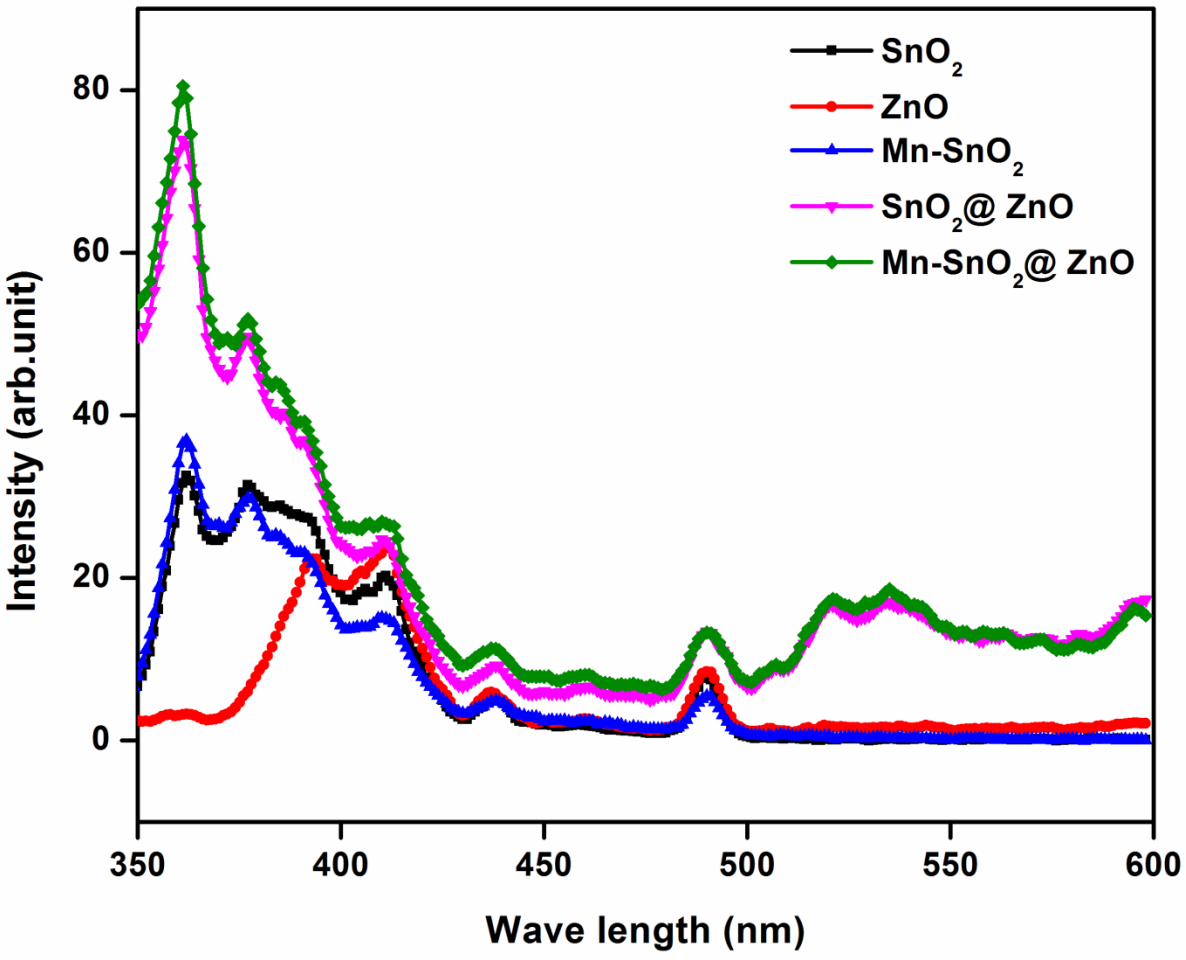

Figure 4 Photoluminescene spectra of synthesized SnO_2, Mn-SnO_2, ZnO, SnO_2@ZnO and Mn-SnO_2@ZnO composite samples.

Field Emission Scanning Electron Microscope analysis

The Field Emission Scanning Electron Microscope (FE-SEM) images of the synthesized SnO_2, ZnO, Mn-SnO_2, SnO_2@ZnO and Mn-SnO_2@ZnO composite samples are shown figure 5 (A-E). The FE-SEM images of the SnO_2, Mn-SnO_2 and ZnO show small spherical grains that are

slightly agglomerated with one another as shown in figure 5 (A-C). The size of the spherical grains are found to be around 16-45 nm. When compared to the pure and doped samples, the SnO_2@ZnO and Mn-SnO_2@ZnO composite samples show loosely bound spherical grain morphology as shown in figure 5 (D,E)

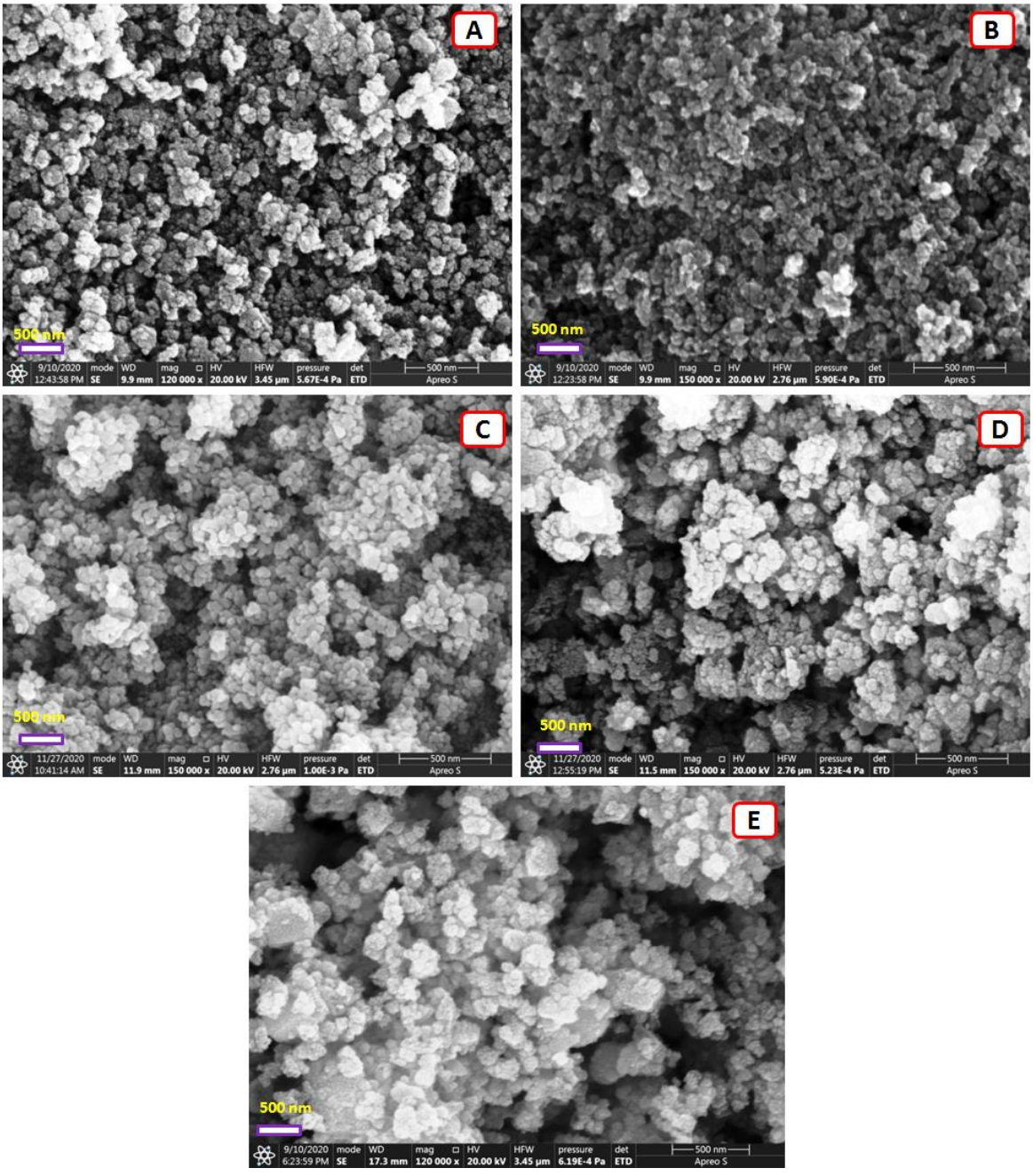

Figure 5 FE-SEM images of synthesized (A) SnO_2, (B) ZnO, (C) Mn-SnO_2, (D) SnO_2@ZnO and (E) Mn-SnO_2@ZnO composite samples.

EDS and element mapping analyses

Figure 6 displays the EDS spectra of the synthesized SnO_2, Mn-SnO_2, ZnO, SnO_2@ZnO and Mn-SnO_2@ZnO composite samples. In the EDS spectra of the SnO_2 and ZnO, the presence of only Sn, O, and Zn, O atoms are observed, respectively, as shown in figure 6(A,B). The Sn, Zn and O atoms are present in the SnO_2@ZnO and along with Mn in the Mn-SnO_2@ZnO composites, respectively, as shown in figure 6(C-E). No other impurity atoms were identified in the synthesized samples which affirm the purity of the synthesized materials. The obtained atomic percentage and weight percentage of the elements are inserted in the corresponding EDS spectra.

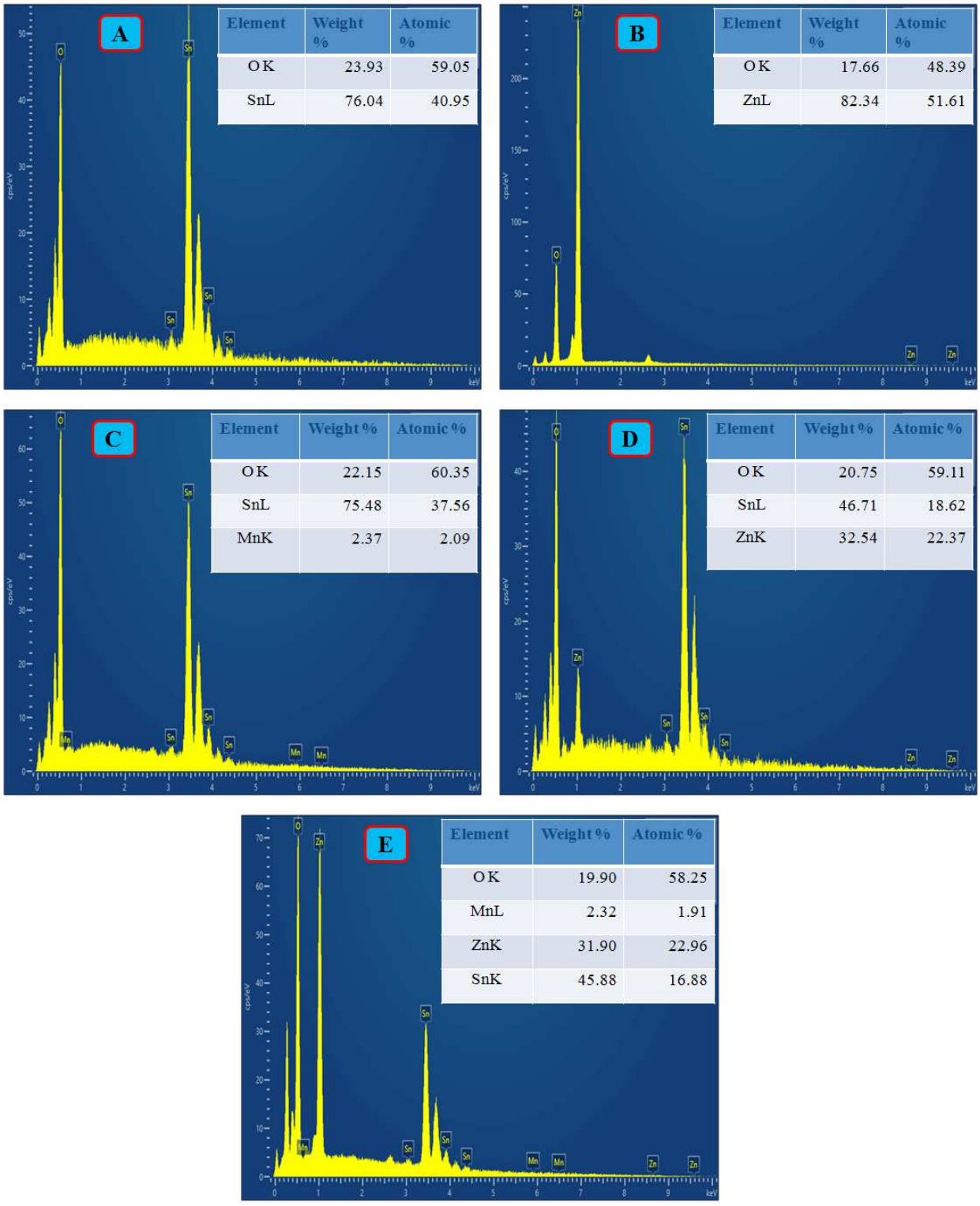

Figure 6 EDS spectra of the synthesized (A) SnO_2, (B) ZnO, (C) Mn-SnO_2, (D) SnO_2@ZnO and (E) Mn-SnO_2@ZnO composite samples.

The element mapping images of the synthesized samples are shown in figure 7. The mapping images also confirm the purity of the samples. Moreover, the observed elements are appeared on the entire surface of the materials.

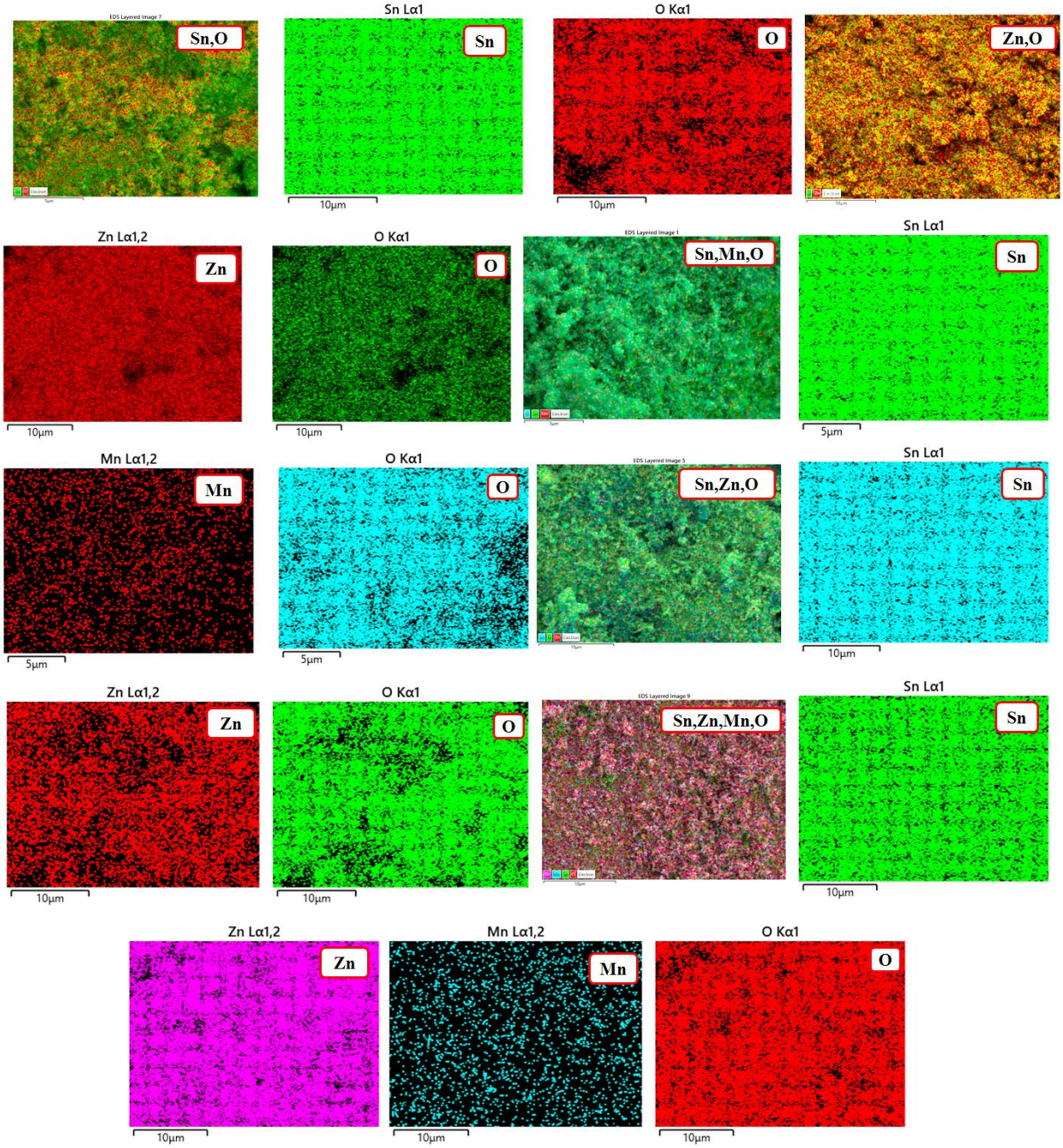

Figure 7 Element mapping of the synthesized SnO2, ZnO, Mn-SnO_2, SnO_2@ZnO and Mn-SnO_2@ZnO composite samples.

X-ray photoelectron spectroscopy analysis

The X-ray photoelectron spectra (XPS) revealed the presence of binding energy peaks of Sn, Zn, O and Mn for SnO_2@ZnO and Mn-SnO_2@ZnO composites and are displayed in figure 8 (A-E). As shown figure 8 (B), the two obvious peaks of Sn, Sn $3d_{5/2}$ and Sn $3d_{3/2}$ are seen at 485.3 eV and 493.7 eV, respectively, which confirm the Sn^{4+} state of Sn [34]. The Zn 2p core level spectra is shown in figure 8(C) which contain two peaks positioned at 1020.5 eV and 1043.8 eV and these peaks correspond to Zn $2p_{3/2}$ and Zn $2p_{1/2}$, respectively. This confirms the Zn^{2+} state of Zn [35]. Furthermore, the wide scan spectra of Mn2p related peaks are exhibited at 642.7 eV and 654.8 eV which correspond to Mn $2p_{3/2}$ and Mn $2p_{1/2}$ respectively. The binding energy difference between the Mn $2p_{3/2}$ and Mn $2p_{1/2}$ is 11.5 eV which confirms the Mn^{4+} state of Mn (see figure 8(D)) [36]. As shown in figure 8 (E), in the case of SnO_2@ZnO and Mn-SnO_2@ZnO composites, the oxygen (O 1*s*) peak is positioned at 529.3 eV which relates to the Sn-O-Sn lattice and the another peak at 530.6 eV corresponds to the adsorbed O_X^- ions (O^- and O^{2-} ions). No other impurity phase elements were determined in the synthesized composite samples and also the obtained results agree well with the PXRD and the EDS results.

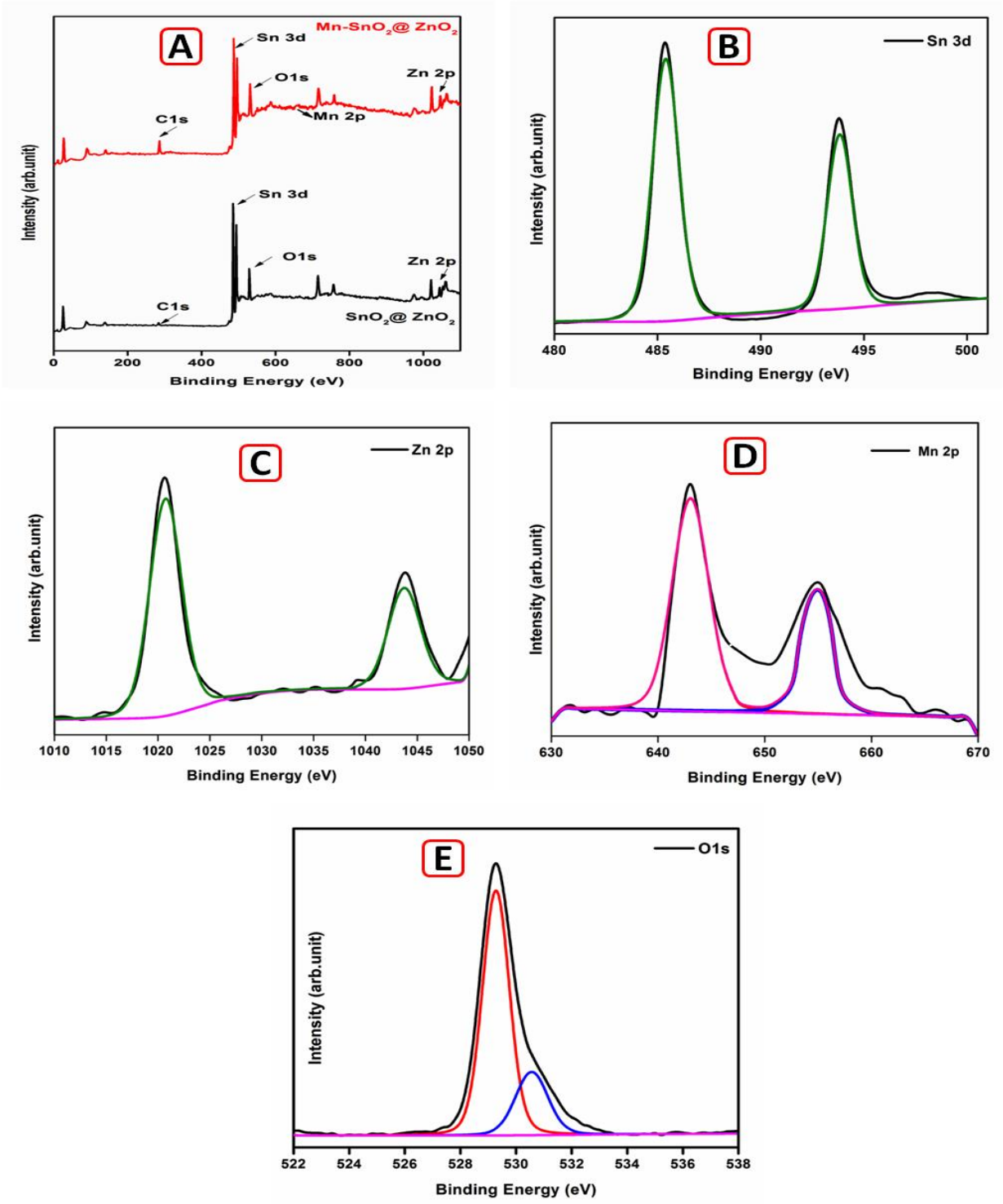

Figure 8 (A) Survey spectrum of SnO_2@ZnO and Mn-SnO_2@ZnO samples, (B-E) Wide scan spectra of Sn3d, Zn2p, Mn2p and O1s levels, respectively.

Photocatalytic performance analysis

The photocatalytic performance of the synthesized SnO_2, Mn-SnO_2, ZnO, SnO_2@ZnO and Mn-SnO_2@ZnO composite samples were studied using methylene blue (MB) and rhodamine B (RhB) dye under visible light irradiation. In the absence of photocatalyst, negligible changes were observed in the MB and RhB dyes after 80 min of visible light irradiation. Up on the addition of the synthesized SnO_2, Mn-SnO_2, ZnO, SnO_2@ZnO and Mn-SnO_2@ZnO photo-catalysts, the major intensity peaks of MB and RhB found at 664 nm and 554 nm gradually decreased with increasing irradiation time. Among the synthesized catalyst, the Mn-SnO_2@ZnO catalyst almost degrades the entire MB and RhB dyes by 80 min of irradiation and the data are shown in figure 9(A,B). The Photo-degradation efficiency was estimated by using following formula [37].

$$\text{Photo-degradation efficiency, } \eta = (1 - C/C_0) \times 100 \ (\%)$$

where, C_0 is the initial MB dye concentration and C is the dye concentration after irradiation.

The values of degradation efficiency with various photo-catalysts are given in table 1 and the same is plotted in figure 9 (C, D), respectively. Overall, the Mn-SnO_2@ZnO catalyst has been found to exhibit higher degradation efficiency when compared to the SnO_2, Mn-SnO_2, ZnO and SnO_2@ZnO catalysts for the MB and RhB dyes.

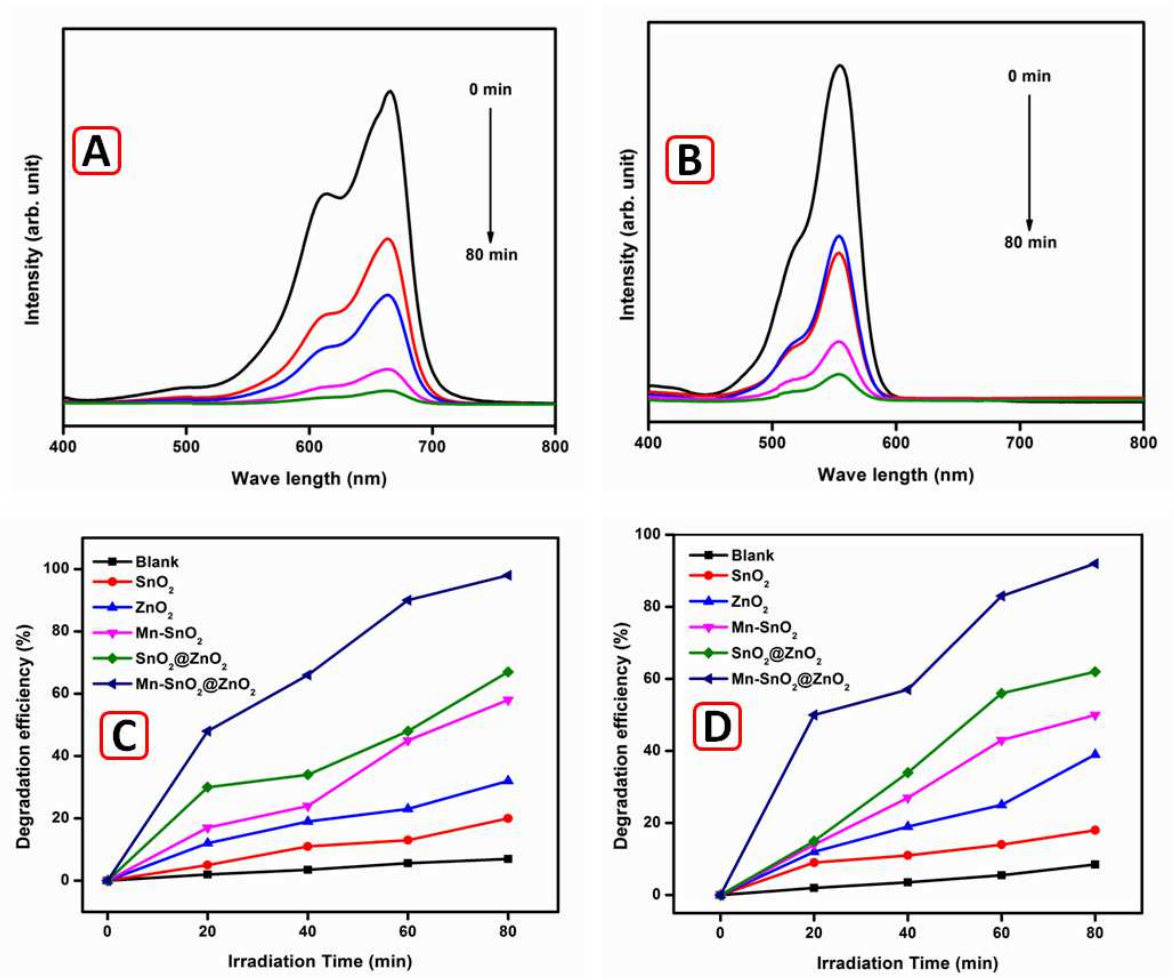

Figure 9 (A,B) The changes in the absorption peaks of MB and RhB dyes for Mn-SnO_2@ZnO catalysts with different irradiation time, (C, D) Photo degradation efficiency of blank, SnO_2, ZnO, Mn-SnO_2, SnO_2@ZnO and Mn-SnO_2@ZnO catalysts using MB and RhB dyes.

The degradation concentration ratio (C/C_0) was calculated for all the synthesized samples and the data is shown in figure 10(A, B). The Mn-SnO_2@ZnO sample was found to exhibit higher C/C_0 when compared to the other photo-catalysts. The rate constant values of the prepared materials were calculated by Langmuir-Hinshelwood model using the following relation:

$$ln\ (C_0/C_t) = kt$$

where C_0 is the initial concentration of dye, C_t is the dye concentration after irradiation for a time period, t and k is the rate constant.

Table 1, The efficiency, rate constant, degradation concentration for the prepared catalyst

Photo-catalyst	Efficiency (%)		Rate Constant (min^{-1})		Degradation Concentration	
	MB	RhB	MB	RhB	MB	RhB
Blank (Without catalyst)	7	8.5	0.006	0.004	0.93	0.91
SnO_2	20	18	0.011	0.015	0.80	0.82
ZnO	32	39	0.013	0.018	0.68	0.61
Mn-SnO_2	58	50	0.030	0.027	0.42	0.50
SnO_2@ZnO	67	62	0.044	0.030	0.33	0.38
Mn-SnO_2@ZnO	98	92	0.077	0.054	0.03	0.08

The rate constant values gradually increased with increasing irradiation time for both MB and RhB dyes. When rate constant values of all the prepared catalyst are compared, the Mn-SnO_2@ZnO catalyst was found to have a high rate constant. The corresponding variations of the rate constant *vs* irradiation time is shown in figure 10 (C, D) and also tabulated in table 1. The lower band gap, large surface area, the formation of heterojunction of Mn-SnO_2 and ZnO helped to increase the separation of photo-generated electrons and holes from recombination process which promoted the photo-catalytic reaction and efficiency of the catalyst.

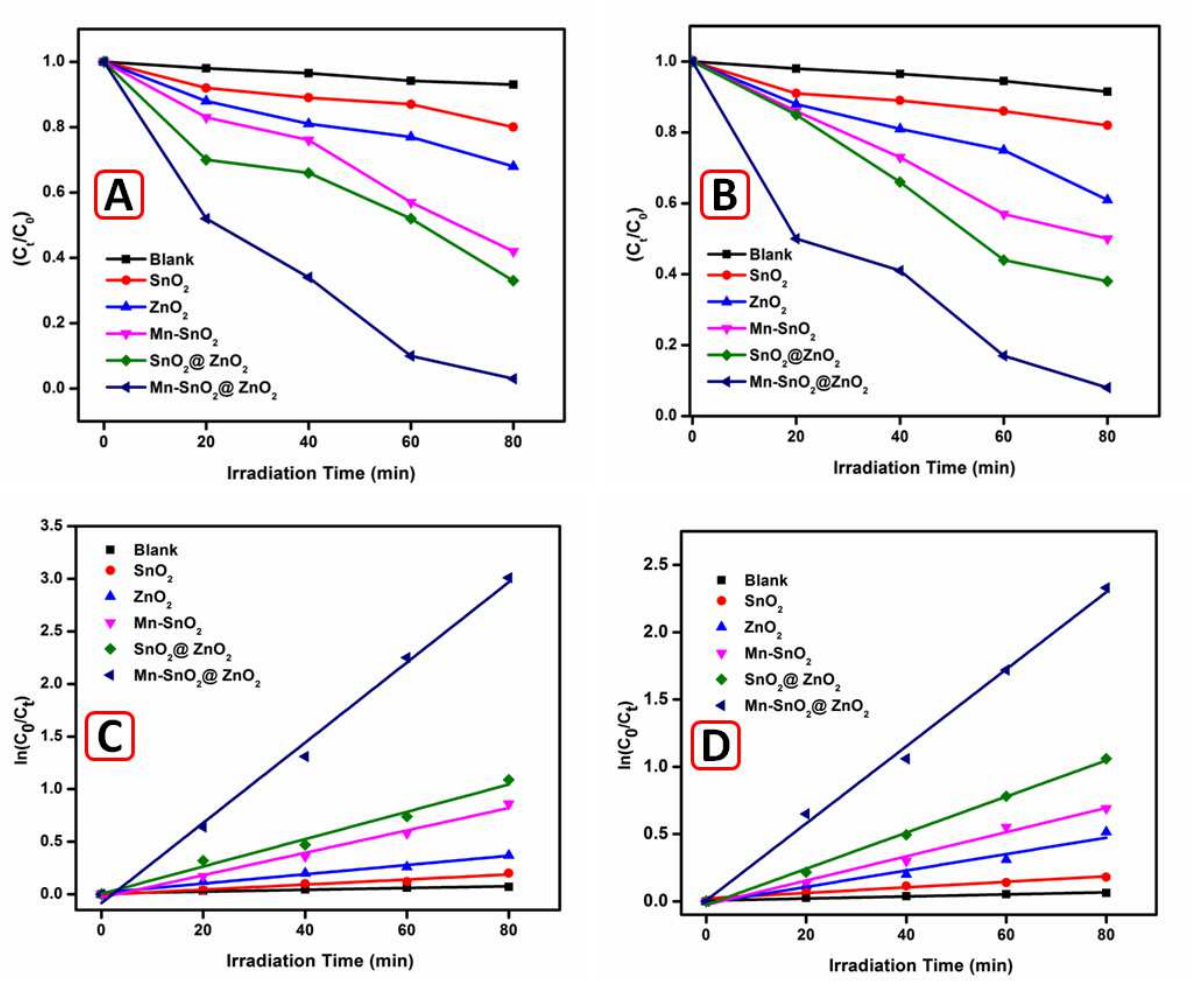

Figure 10 (A,B) Degradation concentration ratio, (C, D) Kinetic study of the blank (no catalyst), SnO_2, Mn-SnO_2, ZnO, SnO_2@ZnO and Mn-SnO_2@ZnO catalysts using MB and RhB dyes with different irradiation time.

The stability test is an important phenomenon which determines the reusability of the prepared material. The Mn-SnO_2@ZnO photo-catalyst was used to conduct the recycling performance analysis against MB and RhB dyes under visible light irradiation. After three consecutive recycles, the degradation efficiencies of MB and RhB dyes reached 95 and 90 % which is shown in figure 11(A,B). After recycles, the Mn-SnO_2@ZnO photo-catalyst was examined using XRD analysis. The XRD pattern of the recycled catalyst is seen to be similar to that of the unused one and is shown in figure 11(C). The recycle performance analysis revealed

that the Mn-SnO_2@ZnO catalyst has excellent degradation efficiency and it can be used as a photo-catalyst for industries' waste water treatments.

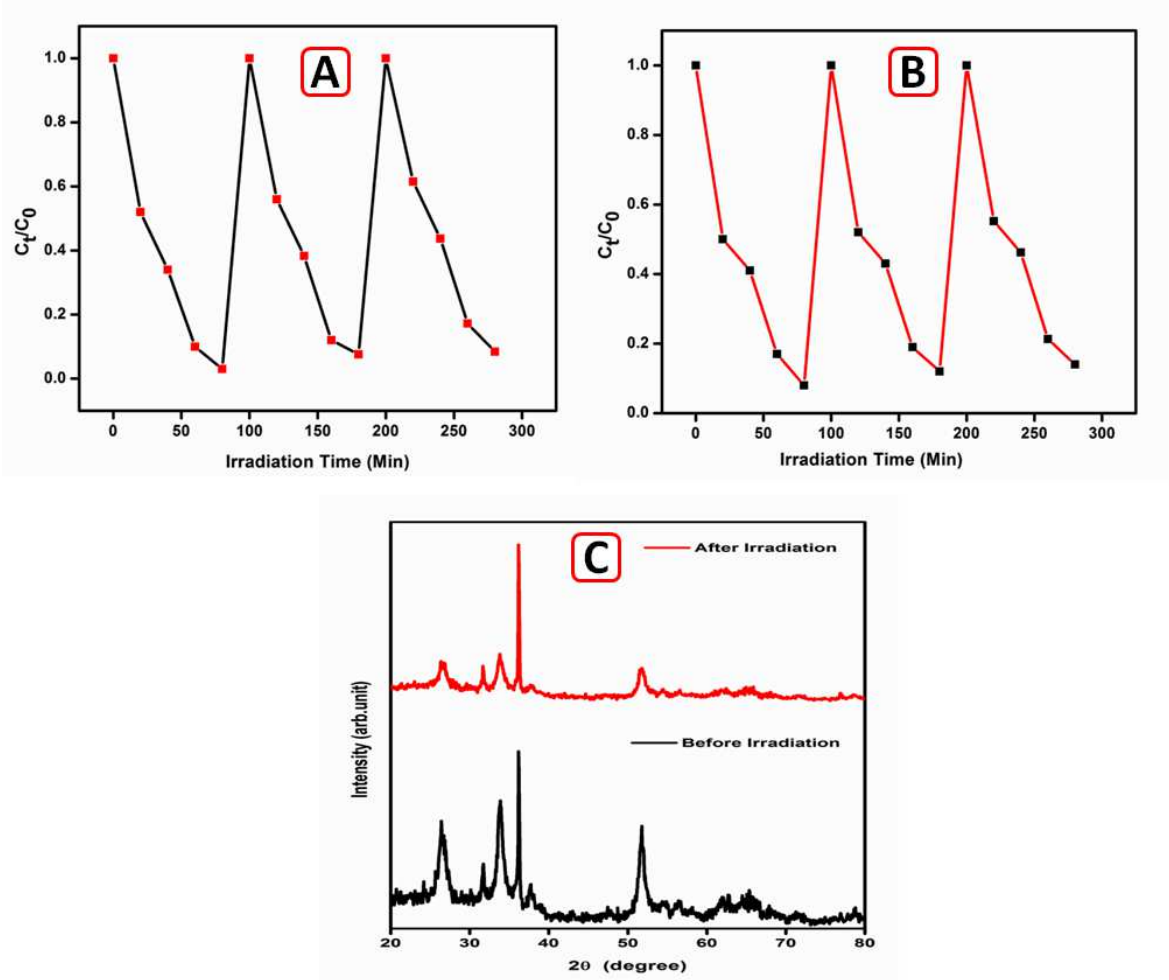

Figure 11(A,B) Mn-SnO_2@ZnO catalyst stability against MB and RhB dyes upon cyclic irradiation of 80 min duration, (B) The XRD patterns of Mn-SnO_2@ZnO photo-catalyst before and after the photocatalytic reaction.

Photocatalytic mechanism

The photo-catalytic performances were analyzed for the SnO_2, Mn-SnO_2, ZnO, SnO_2@ZnO and Mn-SnO_2@ZnO catalysts under visible light irradiation using MB and RhB organic dyes. Among the catalyst, the Mn-SnO_2@ZnO was found to exhibit higher degradation efficiency for both the MB and RhB dyes. The enhanced photocatalytic activity was observed for the Mn-SnO_2@ZnO catalyst due to the coupling of semiconductors with different band gaps

which favours for the electron hole separation. Due to more electron hole separation, the enriched photocatalytic activity was identified for the Mn-SnO_2@ZnO which is based on the band alignment. Further, the semiconductors band edge potential level plays a vital role in determining the flow of photo-excited charge carriers. The band edge potentials of conduction and valance band of SnO_2, Mn-SnO_2 and ZnO were calculated by using the below relations:

$$E_{VB} = X - E_e + 0.5\, E_g$$

$$E_{CB} = E_{VB} - E_g$$

where, E_{VB} is the valence band edge potential, E_{CB} is the conduction band edge potential, X is the electro-negativity of the semiconductors SnO_2 and ZnO (6.0 and 5.79 eV), E_e is the energy of free electrons on the hydrogen scale (4.50 eV), E_g is energy band gap (SnO_2: 3.52 eV, Mn-SnO_2: 3.32eV and ZnO: 3.01 eV). The valance band edge potential (E_{VB}) was found to be 3.26 eV, 3.16 eV and 2.795 eV and conduction band edge potential (E_{CB}) was found at -0.26 eV, -0.16 eV and -0.21 eV for the SnO_2, Mn-SnO_2 and ZnO catalysts, respectively. Figure 12(A) shows the charge transfer schematic mechanism of the prepared Mn-SnO_2@ZnO catalyst. When visible light pass through the Mn-SnO_2@ZnO hetero-structure, the electrons from the valence band are excited to the conduction band of the Mn-SnO_2 and ZnO and simultaneously holes are generated in the valance band. The photo generated electrons moved from higher energetically ZnO CB edge to lower CB edge of Mn-SnO_2 and holes are moved in the opposite side due to the appropriate valance band position. Thus, photo-generated electrons and holes were vertically moved to Mn-SnO_2 and ZnO which gives higher charge separation and lower charge recombination. The higher charge separation also helped to enhance the charge carrier life time and also enrich the interfacial charge transfer to adsorbed surface of the organic pollutants which helped to enhance the photocatalytic performance of the Mn-SnO_2@ZnO composite.

A possible reaction mechanism is proposed as follows:

$$\mathrm{Mn - SnO_2} + h\nu \rightarrow \mathrm{h^+(ZnO) + e^-(Mn - SnO_2)}$$

$$\mathrm{O_2 + e^- \rightarrow \cdot O_2^-}$$

$$\mathrm{\cdot O_2^- + H_2O \rightarrow HO_2^{\cdot -} + OH^-}$$

$$\mathrm{HO_2^{\cdot -} + H_2O \rightarrow H_2O_2 + OH^+}$$

$$\mathrm{H_2O_2 \rightarrow 2OH^{\cdot}}$$

$$h^+ + OH^- \rightarrow \cdot OH$$

$$\cdot OH + MB \rightarrow Degradation\ Products$$

The electron in the conduction band of SnO_2 reacts with oxygen adsorbed on the surface of SnO_2 to generate superoxide radials anion ($\cdot O_2^-$). These $\cdot O_2^-$ radical further react with H_2O to produce the $\cdot OH$ radical. Simultaneously, holes (h^+) migrated to ZnO react with H_2O to produce hydroxyl ($\cdot OH$) radical spices and the radicals degrade the MB and RhB dyes with degradation products of CO_2 and water [38]. The trapping experiment was conducted by using benzoquinone (BQ), ethylenediamine tetra acetic acid disodium (EDTA), and isopropanol (IPA) as an O^{2-}, h^+ and $\cdot OH$ radical scavengers respectively.

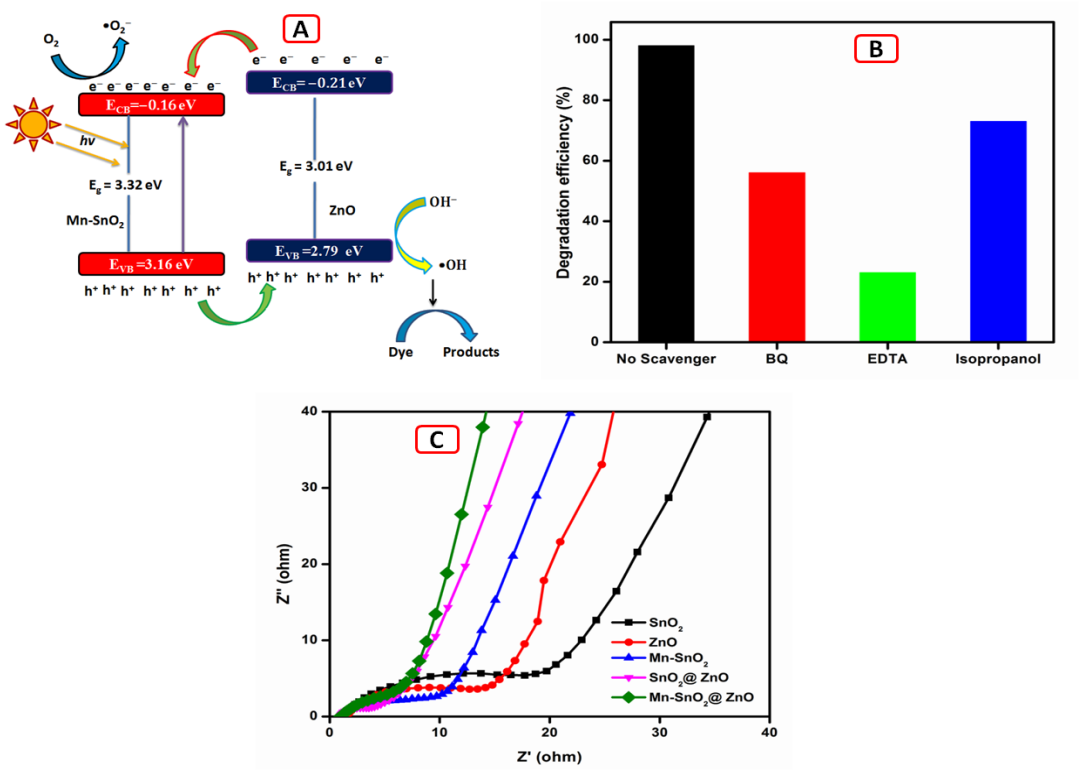

Figure 12 (A) Schematic diagram of the catalytic mechanism of Mn-SnO_2@ZnO photo-catalyst, (B) Trapping experiment for the Mn-SnO_2@ZnO photo-catalyst using MB dye, (C) EIS spectra of SnO_2, ZnO, Mn-SnO_2, SnO_2@ZnO and Mn-SnO_2@ZnO samples.

The scavenger experiment results are shown in figure 12 (B). The result clearly revealed that BQ, EDTA, IPA reduce the photo-degradation efficiency under the visible light irradiation

and also it confirms the superoxide and hydroxyl radicals are the important reactive species of the dye degradation process under the visible light irradiation. Apart from this, the EIS spectra also confirm the charge transfer and the recombination rate between the holes and photo-generated electrons. The EIS spectra of all the synthesized samples are shown in figure 12(C). The Mn-SnO_2@ZnO composite has lower solution and charge transfer resistances compared to other catalysts. The charge transfer resistance was found to be 19.7 Ω, 15.6 Ω, 10.7 Ω, 6.2 Ω and 5.7 Ω for the SnO_2, ZnO, Mn-SnO_2, SnO_2@ZnO and Mn-SnO_2@ZnO photo-catalysts, respectively. The EIS spectra confirm that the Mn-SnO_2@ZnO has a higher charge transfer and lower recombination rates which helps to enhance the photocatalytic activity under the visible light irradiation.

Conclusion

In summary, we successfully synthesized Mn-SnO_2@ZnO composite by using a simple chemical co-precipitation method. The structural, optical, morphology, purity, binding energy characteristics and the photocatalytic performances were analyzed for the synthesized samples. The Mn-SnO_2@ZnO heterostructure was found to exhibit higher degradation efficiency when compared to pure SnO_2 and ZnO samples using MB and RhB dyes under visible light irradiation. This is due to the separation of photo-generated electrons and holes and also due to higher charge transfer developed at the interface of the Mn-SnO_2@ZnO. From a detailed photo-catalytic performance analysis, the Mn-SnO_2@ZnO heterostructure has been found as a suitable material for waste water treatment as well as to remove the undesired organic compounds from the environment.

Acknowledgements

S.Asaithambi gratefully acknowledges RUSA 2.0 for awarding Ph.D. fellowship (F.No.Alu/RUSA/Ph.D Fellowships/2019) and G. Ravi greatly acknowledges the DST-SERB (File No. EMR/2017/001999), UGC-SAP (F.530/18/DRS-III/2015), DST-FIST (SR/FST/PSI-202/2015), DST-PURSE (SR/PURSE Phase 2/38 (G)) and RUSA 2.0 (24-51/2014) for financial support to carry out this research work.

Compliance with ethical standards

Conflict of interest The authors declare that they have no conflict of interest

References

[1] M. Sabarinathan, S. Harish, J. Archana, M. Navaneethan, H. Ikeda, Y. Hayakawa, RSC Adv., 7 24754 -24763 (2017) .

[2] S. Sai Guru Srinivasan, B. Govardhanan, P. Aabel, M. Ashok, M.C. Santhosh Kumar, Solar Energy, **187** 368–378 (2019).

[3] A.Fujishima, K. Honda, Nature, **238** 37 –38(1972).

[4] H. Park, H. I. Kim, G. H. Moon and W. Choi, Energy Environ. Sci., **9** 411-433 (2016).

[5] P. Li, Y. Lan, Q. Zhang, Z. Zhao, T. Pullerits, K. Zheng and Y. Zhou, J. Phys. Chem. C., **120** 9253-9262 (2016).

[6] S. Kumar, A. Baruah, S. Tonda, B. Kumar, V. Shanker and B. Sreedhar, Nanoscale, **6** 4830-4842 (2014).

[7] J.C. Colmenares, R. Luque, J.M. Campelo, F. Colmenares, Z. Karpinski, A.A. Romero, Materials, **2** 2228-2258 (2009).

[8] S.S.Wu, H.Q.Cao, S.F.Yin, X.W.Liu and X.R.Zhang, J.Phys.Chem.C, **113** 17893- 17898 (2009).

[9] X. Chen, B. H. Zhou, S. L. Yang, H. S. Wu, Y. Wu, L. Wu, J. Pan and X. Xiong, RSC Adv., **5** 68953- 68963 (2015).

[10] B. Babu, A. Kadam, R. Ravikumar, C. Byon, J. Alloys Compd., **703** 330–336 (2017).

[11] B. Babu, A.N. Kadam, G. Thirumala Rao, Sang-Wha Lee, Chan Byond, Jaesool Shim, Journal of Luminescence, **195** (2018) 283–289.

[12] S.Asaithambi, R.Murugan, P.Sakthivel, M.Karuppaiah, S.Rajendran, G.Ravi, Journal of nanoscience and nanotechnology, **19** 4438-4446 (2019).

[13] S.Asaithambi, P.Sakthivel, M.Karuppaiah, R.Murugan, R.Yuvakkumar, G.Ravi, Journal of electronic materials, **48** 2183-2194 (2019).

[14] W.B.H. Othmen, B. Sieber, C. Cordier, H. Elhouichet, A. Addad, B. Gelloz, M. Moreau, A. Barras, M. Ferid, R. Boukherroub, Mater. Res. Bull. **83** 481–490 (2016).

[15] Q.J. Xiang, J.G. Yu, M. Jaroniec, Chem. Soc. Rev., **41** 782 –796 (2012).

[16] H. Xia, H. Zhuang, T. Zhang, D. Xiao, Mater. Lett. **62** 1126-1128 (2008).

[17] HL.Xia, HS.Zhuang, T. Zhang, DC.Xiao, J Environ Sci., **19** 1141-1145 (2007).

[18] S.H.Hwang, C.Kim, J.Jang, Catal. Commun., **12** 1037-1041(2011).

[19] C. Zhu, Y. Li, Q. Su, B. Lu, J. Pan, J. Zhang, E. Xie, W. Lan, J Alloys Compd., **575** 333-338 (2013).

[20] H.R. Pouretedal, Z. Tofangsazi, M.H. Keshavarz, J. Alloys. Compd., **513** 359– 364 (2012).

[21] A. Priyadharsan, V. Vasanthakumar, S. Karthikeyan, V. Raj, S. Shanavas, P.M. Anbarasan, J. Photochem. Photobiol., A., **346** 32–45 (2017).

[22] M.A. Subhan, T. Ahmed, N. Uddin, M.A.K. Azad and K. Begum, Spectrochim. Acta, Part A., **136** 824–831 (2015).

[23] P. Senthil Kumar, M. Selvakumar, S. Ganesh Babu, S. Induja, S. Karuthapandian, J. Alloy. Compd., **701** 562-573 (2017).

[24] Jiaojiao Lin, Zhanzhou Luo, Jiaojiao Liu, Ping Li, Materials Science in Semiconductor Processing, **87** 24–31 (2018).

[25] H. F. Moafi, M. A. Zanjanchi and A. F. Shojaie, Materials Chemistry and Physics, **139** (2013) 856-864.

[26] Z.M. Tian, S.L. Yuan, J.H. He, P. Li, S.Q. Zhang, C.H. Wang, Y.Q. Wang, S.Y. Yin, L. Liu, J. Alloy. Compd., **466** 26-30 (2008).

[27] M. Batzill, U. Diebold, Prog. Surf. Sci., **79** 47-154 (2005).

[28] G.Vijayaprasath, R.Murugan, S.Asaithambi, G.Anandha Babu, P.Sakthivel, T.Mahalingam, Y.Hayakawa, G.Ravi, Appl. Phys. A, 122:122(2016).

[29] T. Shrividhya, G. Ravi, Y.Hayakawa, T.Mahalingam, J Mater Sci: Mater Electron., **25** 3885–3894 (2014).

[30] S.Asaithambi, P.Sakthivel, M.Karuppaiah, Y.Hayakawa, A.Loganathan, G.Ravi, Applied Physics A, 126:265 (2020).

[31] G. Vijayaprasath, R. Murugan, S. Asaithambi, P. Sakthivel, T. Mahalingam, Y. Hayakawa, G. Ravi, Ceramics International, **42** 2836-2845(2016).

[32] G. Vijayaprasath, R. Murugan, T. Mahalingam, Y. Hayakawa, G. Ravi, Journal of Alloys and Compounds, **649** 275-284 (2015).

[33] G.Vijayaprasath, R.Murugan, Y.Hayakawa, G.Ravi, Journal of Luminescence, **178** 375-383 (2016).

[34] K. Mallikarjuna, Gazi A.K.M. Rafiqul Bari, S.V.Prabhakar Vattikuti, Haekyoung Kim, , International journal of hydrogen energy, **45** 32789-32796 (2020).

[35] X.J Wang, W.Wang, Y.L.Liu, Sens. Actuators, B., **168** 39 −45 (2012).

[36] Q. Li, G. Li, C. Fu, D. Luo, J. Fan, D. Xie, L. Li, J.Mater. Chem. A., **3** 10592-10602 (2015).

[37] S Asaithambi, P Sakthivel, M Karuppaiah, K Balamurugan, R Yuvakkumar, M Thambidurai, G Ravi, J. Alloys. Compds, **853** 157060 (2021).

[38] Md. Tamez Uddin, Md. Enamul Hoque, M.C. Bhoumick, RSC Adv., **10** 23554 (2020).

Figures

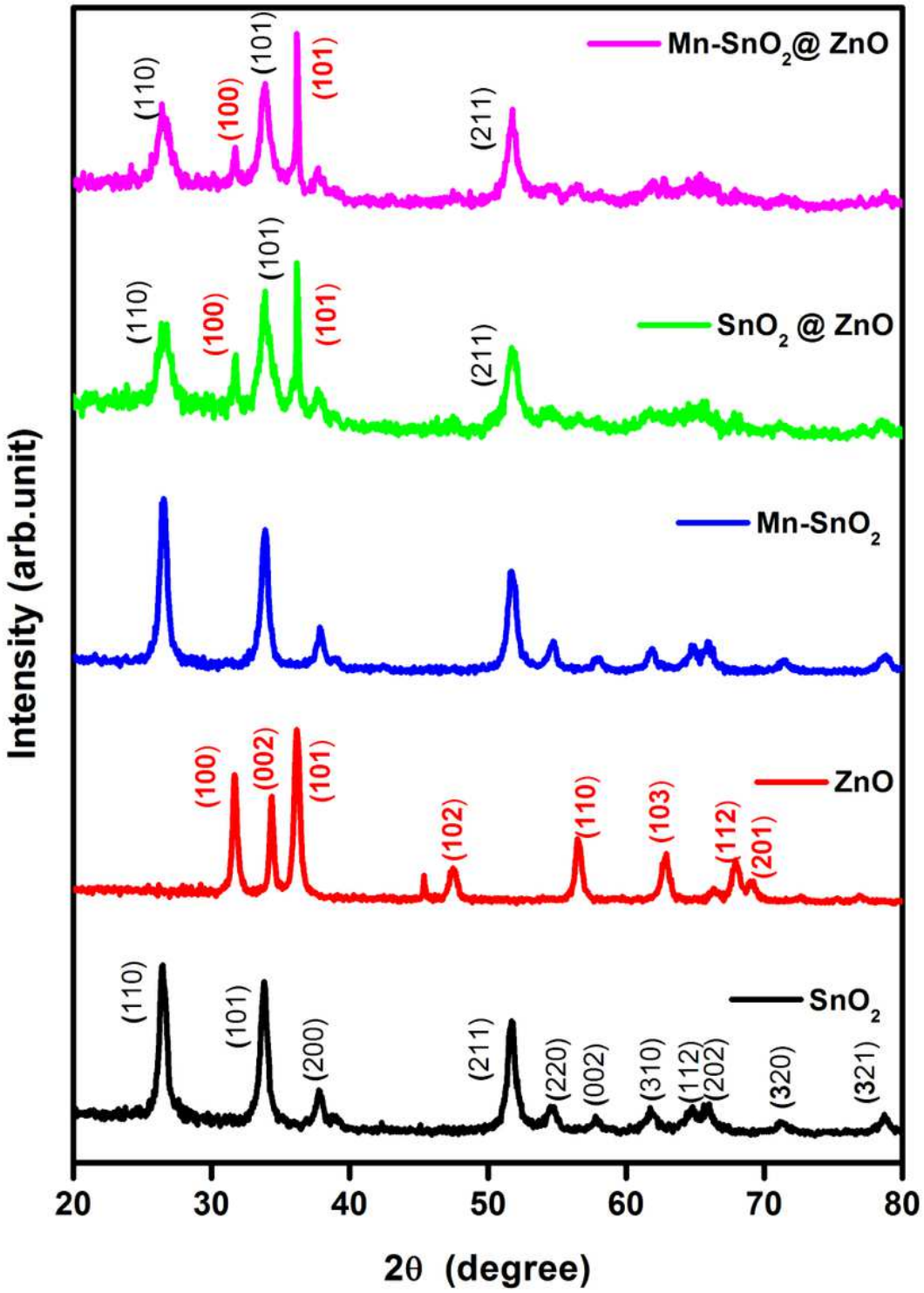

Figure 1

PXRD pattern of synthesized SnO2, ZnO, Mn-SnO2, SnO2@ZnO and Mn-SnO2@ZnO composite samples.

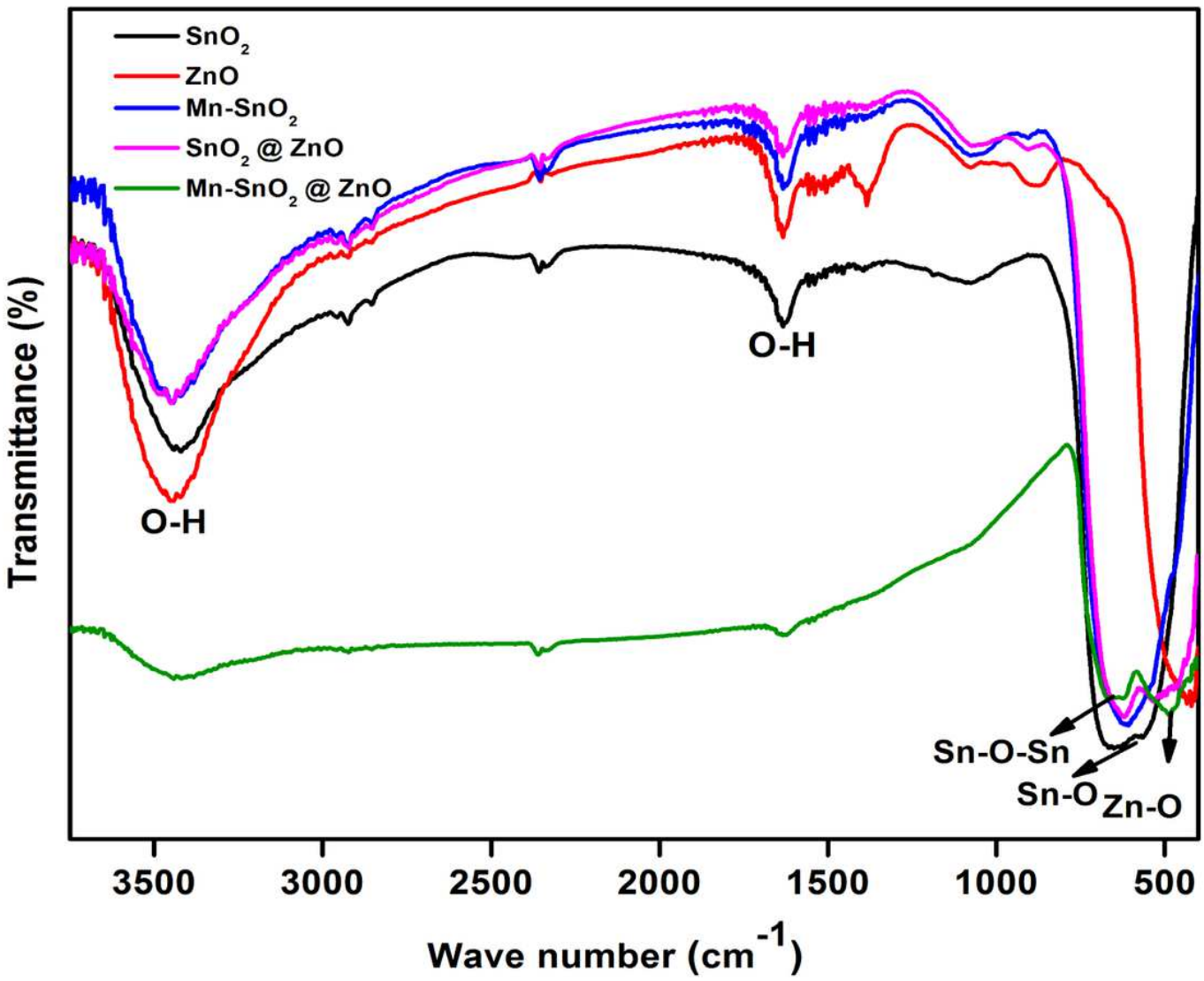

Figure 2

FTIR spectra of the synthesized SnO2, Mn-SnO2, ZnO, SnO2@ZnO and Mn-SnO2@ZnO composites samples.

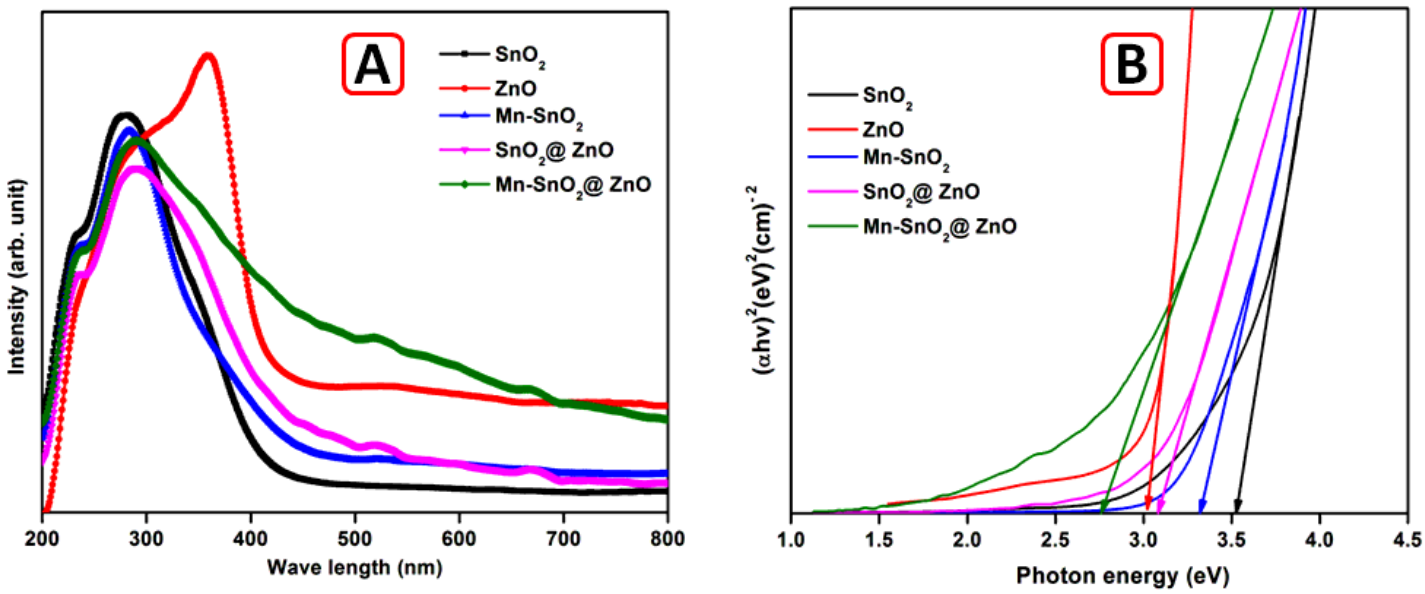

Figure 3

(A) UV-visible absorption spectra, (B) Tauc plots of synthesized SnO2, Mn-SnO2, ZnO, SnO2@ZnO and Mn-SnO2@ZnO composite samples.

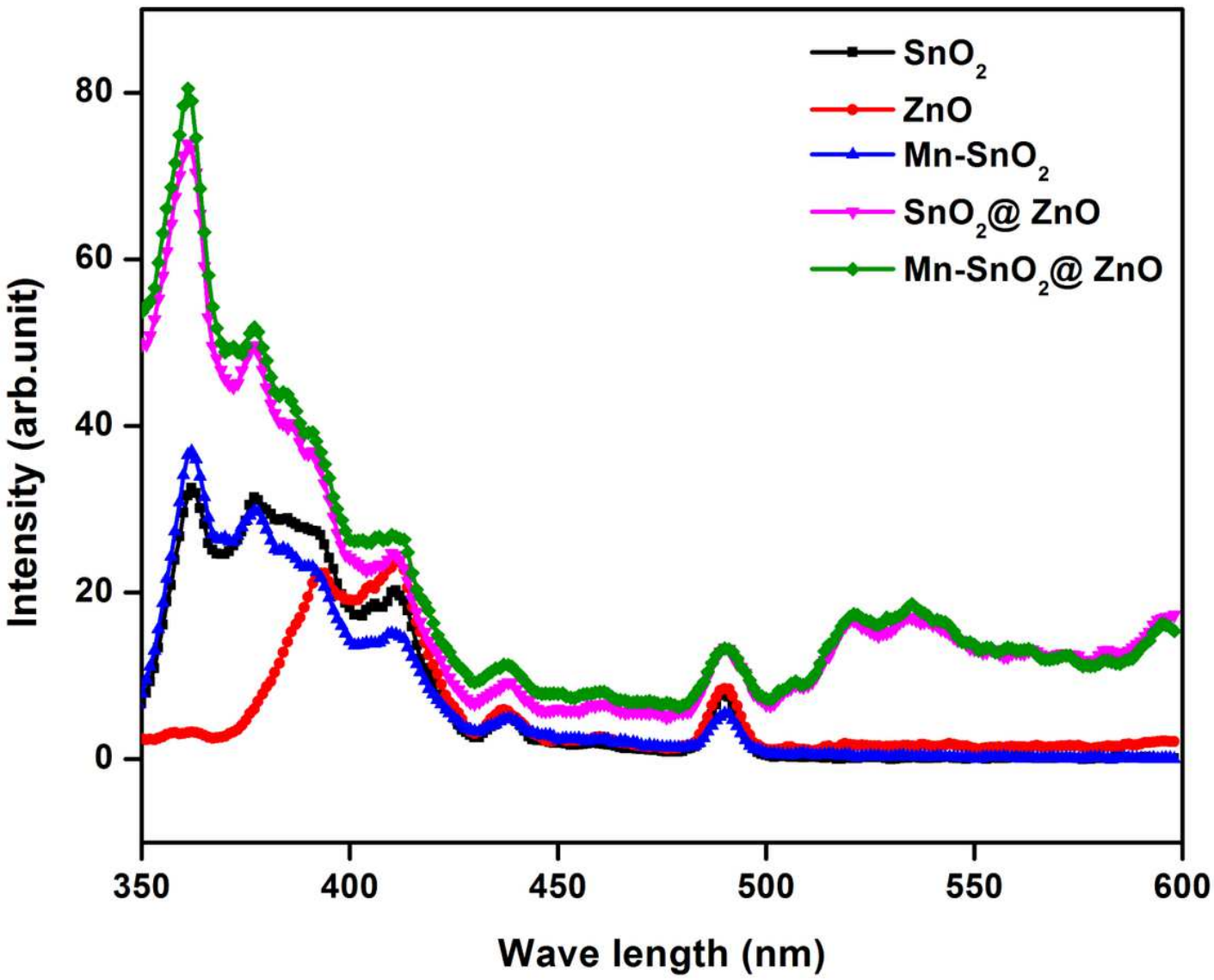

Figure 4

Photoluminescene spectra of synthesized SnO2, Mn-SnO2, ZnO, SnO2@ZnO and Mn-SnO2@ZnO composite samples.

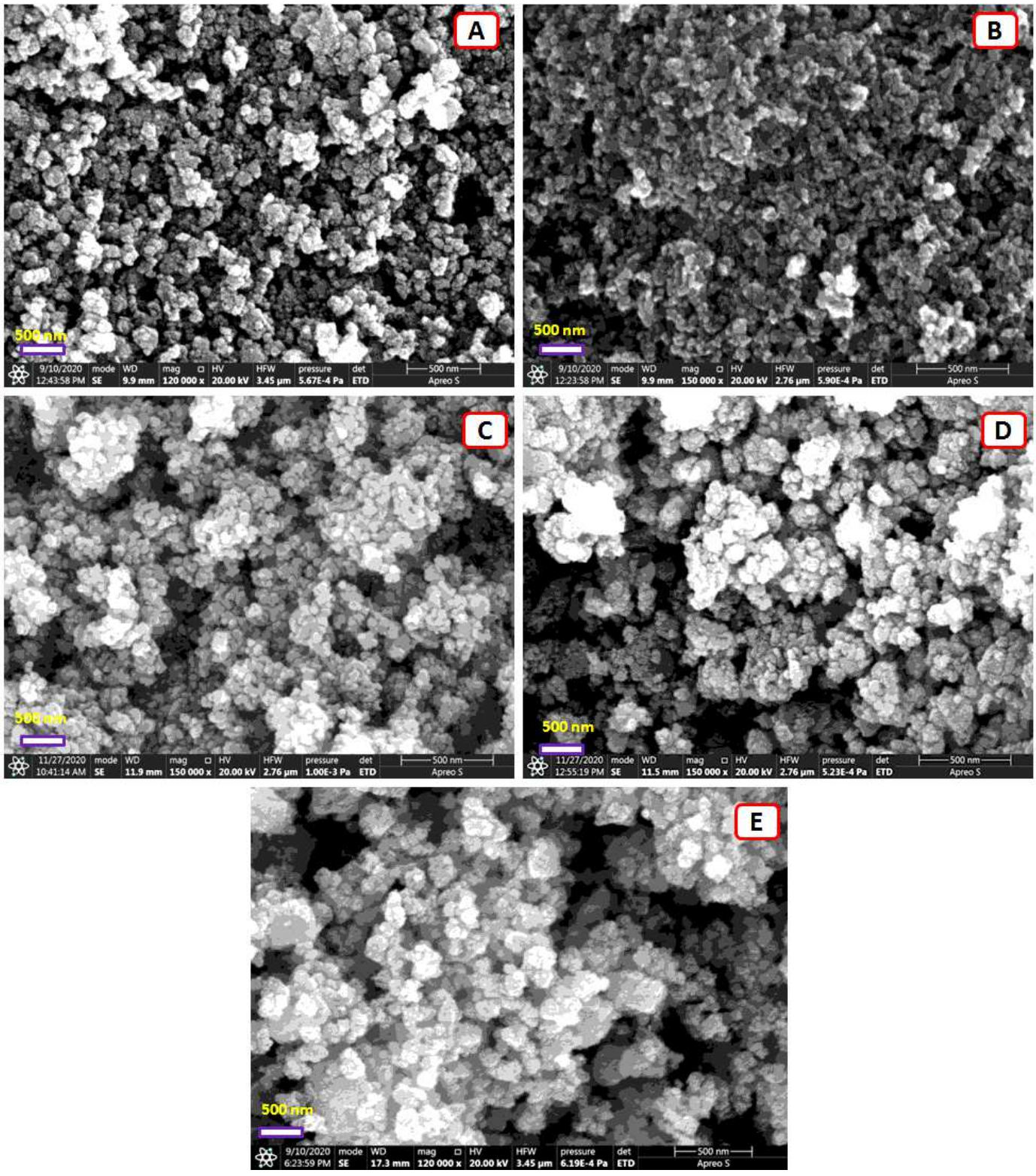

Figure 5

FE-SEM images of synthesized (A) SnO2, (B) ZnO, (C) Mn-SnO2, (D) SnO2@ZnO and (E) Mn-SnO2@ZnO composite samples.

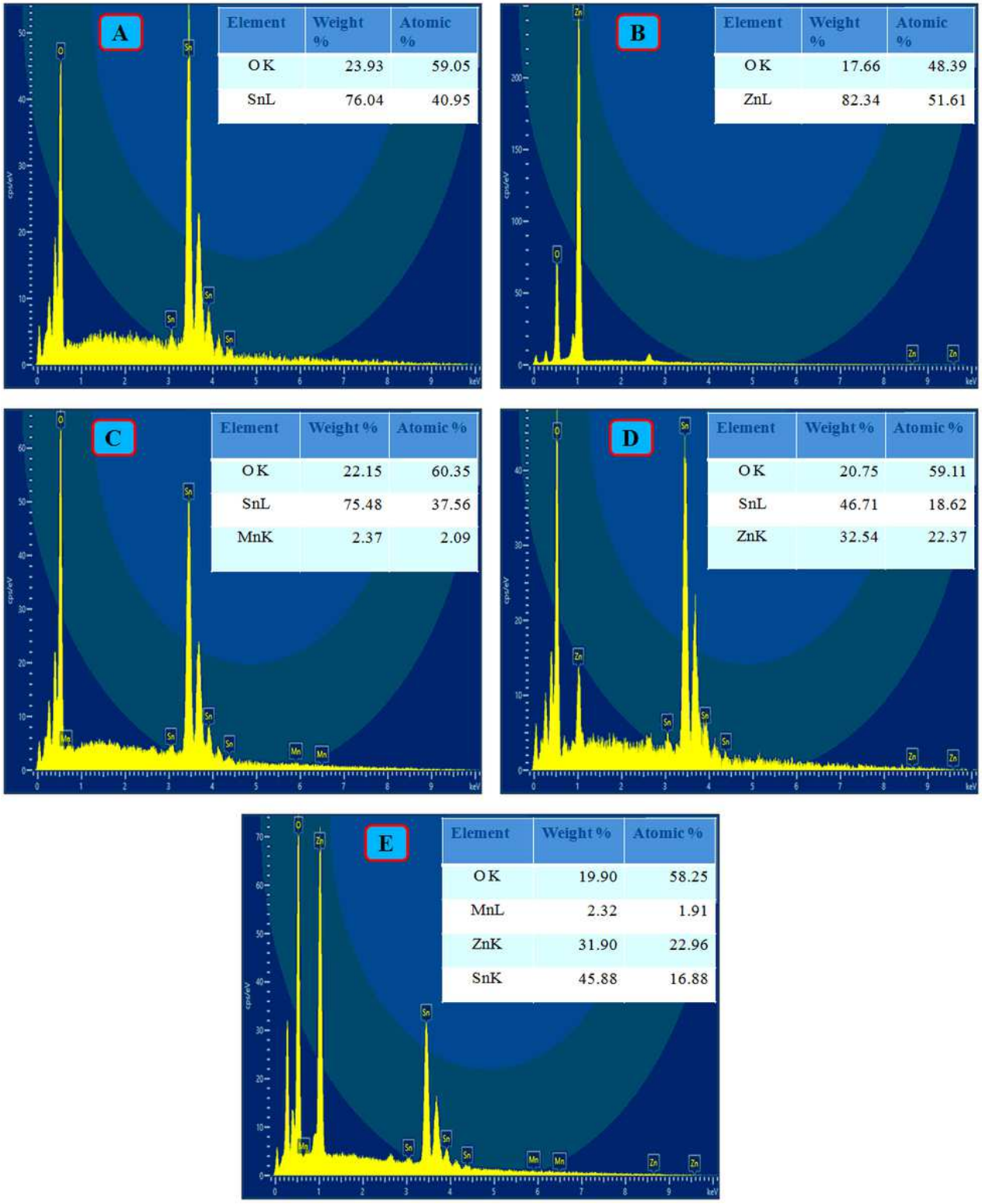

Figure 6

EDS spectra of the synthesized (A) SnO2, (B) ZnO, (C) Mn-SnO2, (D) SnO2@ZnO and (E) Mn-SnO2@ZnO composite samples.

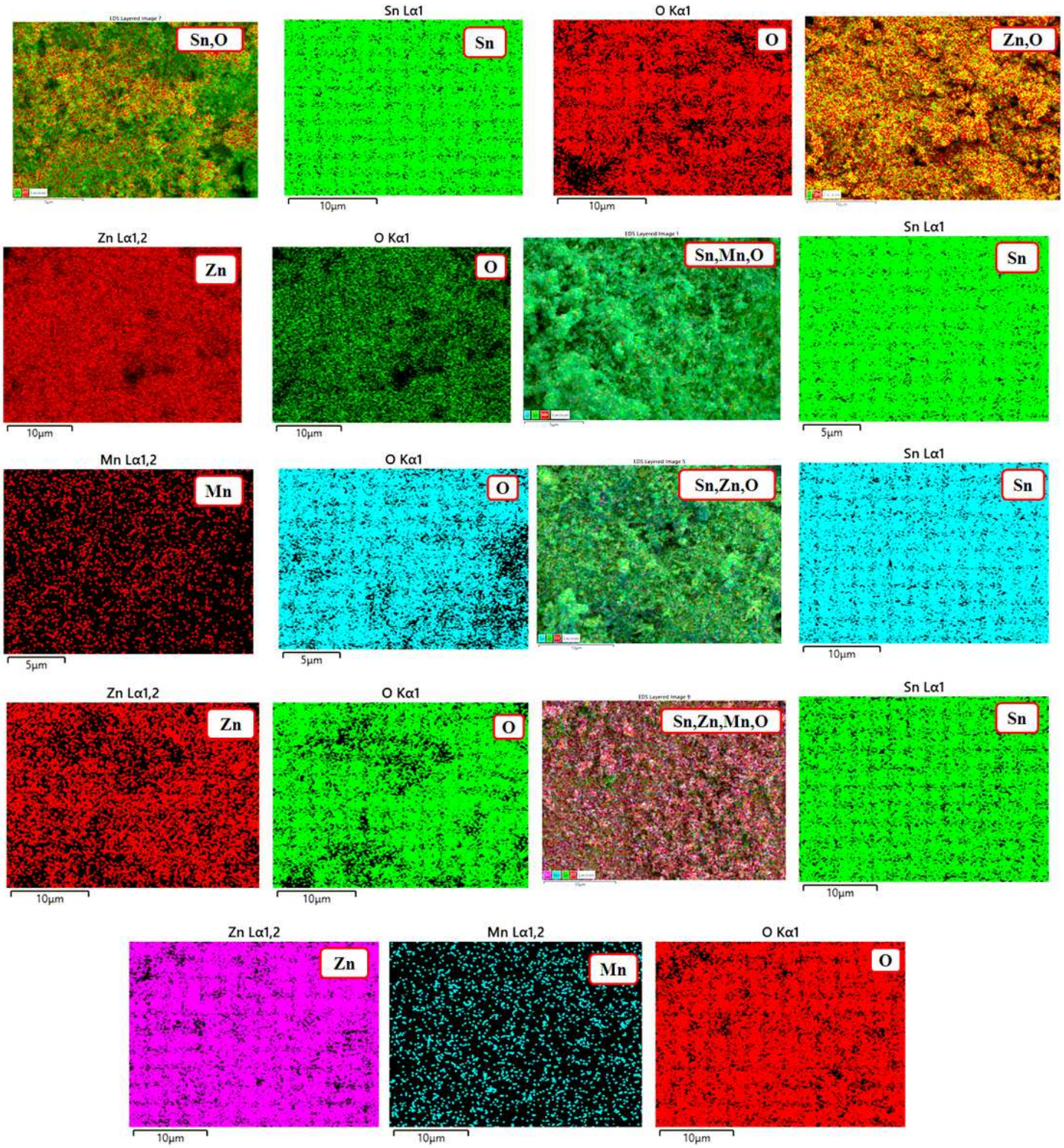

Figure 7

Element mapping of the synthesized SnO2, ZnO, Mn-SnO2, SnO2@ZnO and Mn-SnO2@ZnO composite samples.

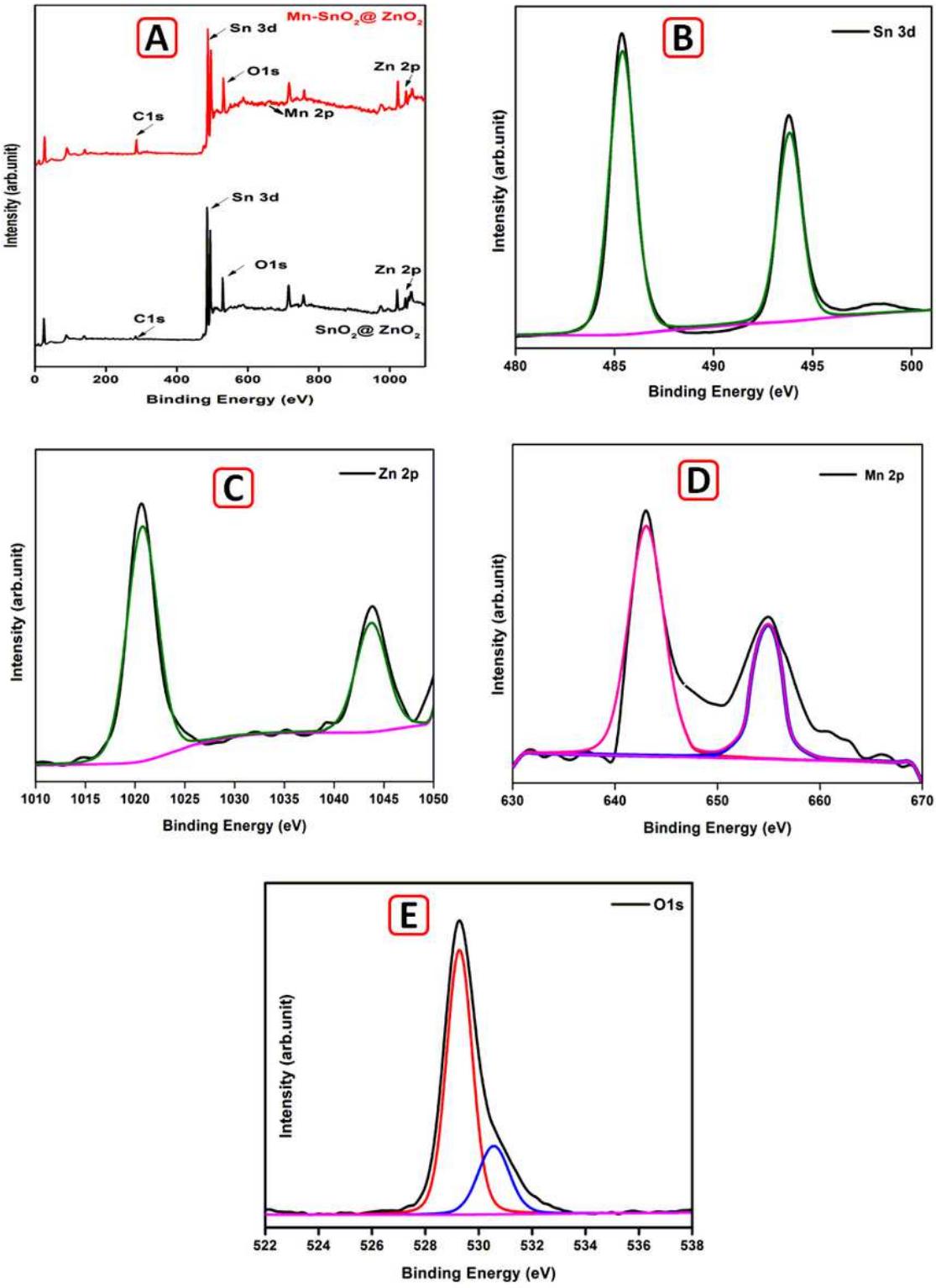

Figure 8

(A) Survey spectrum of SnO2@ZnO and Mn-SnO2@ZnO samples, (B-E) Wide scan spectra of Sn3d, Zn2p, Mn2p and O1s levels, respectively.

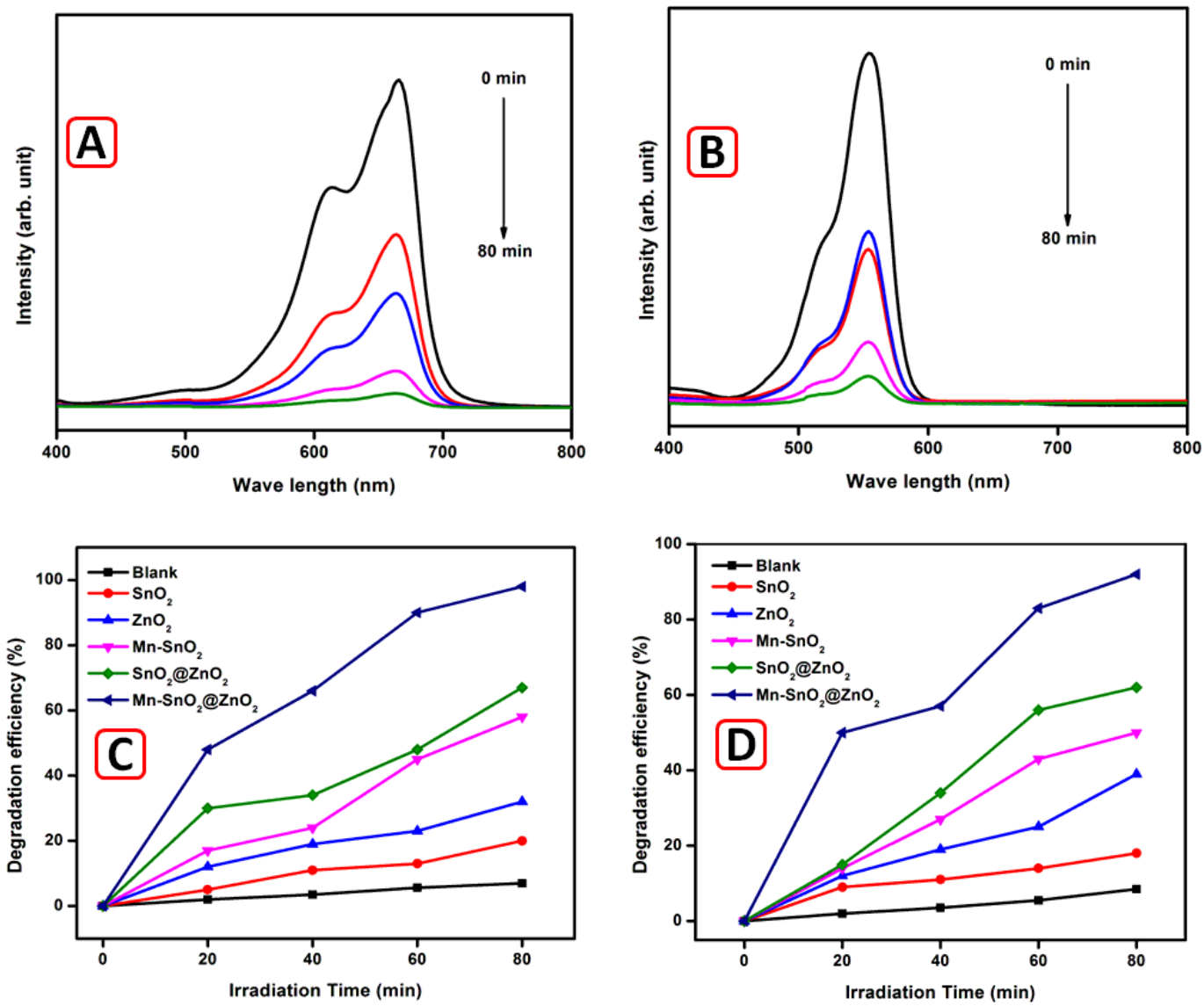

Figure 9

(A,B) The changes in the absorption peaks of MB and RhB dyes for Mn-SnO2@ZnO catalysts with different irradiation time, (C, D) Photo degradation efficiency of blank, SnO2, ZnO, Mn-SnO2, SnO2@ZnO and Mn-SnO2@ZnO catalysts using MB and RhB dyes.

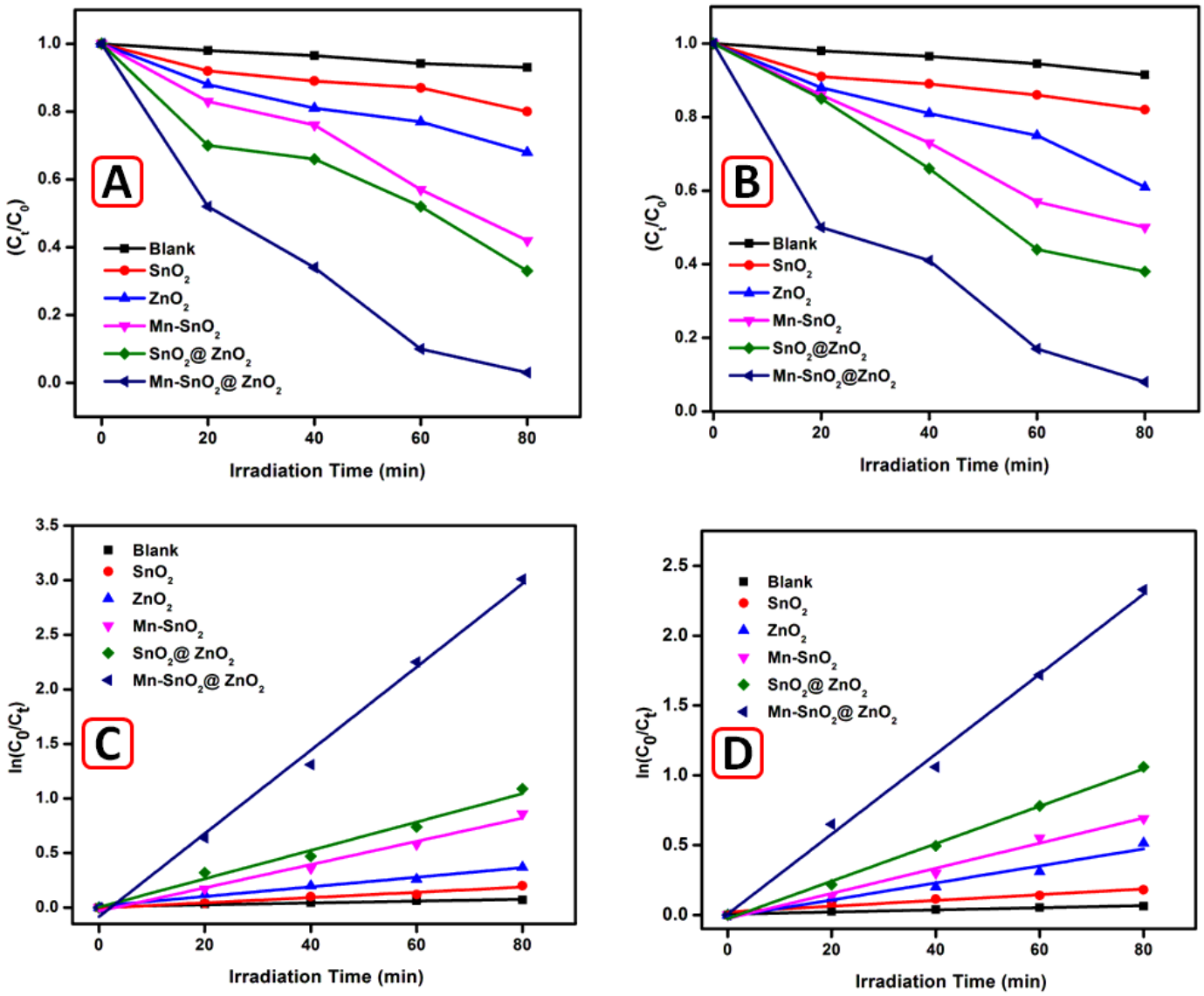

Figure 10

(A,B) Degradation concentration ratio, (C, D) Kinetic study of the blank (no catalyst), SnO2, Mn-SnO2, ZnO, SnO2@ZnO and Mn-SnO2@ZnO catalysts using MB and RhB dyes with different irradiation time.

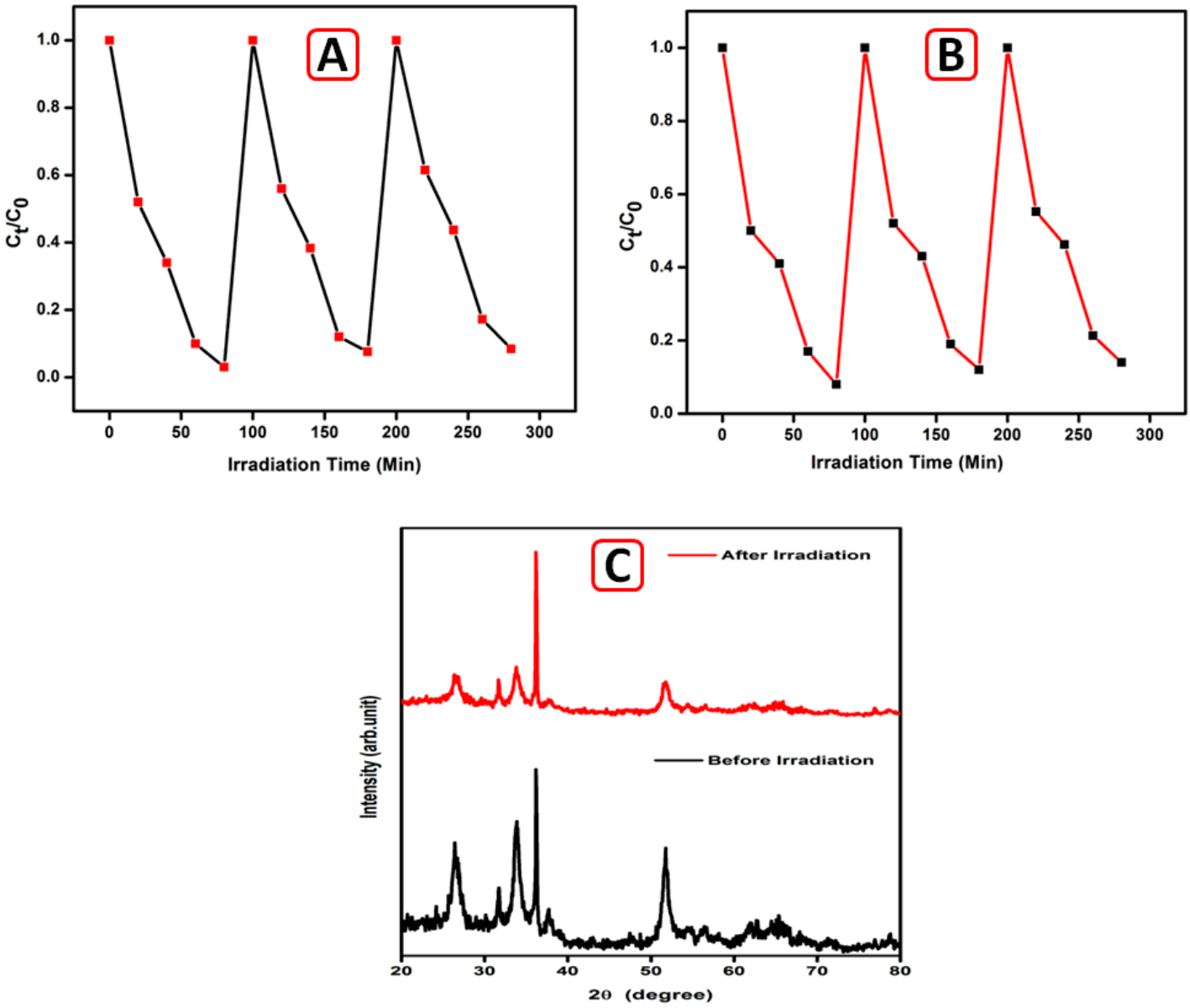

Figure 11

(A,B) Mn-SnO2@ZnO catalyst stability against MB and RhB dyes upon cyclic irradiation of 80 min duration, (B) The XRD patterns of Mn-SnO2@ZnO photo-catalyst before and after the photocatalytic reaction.

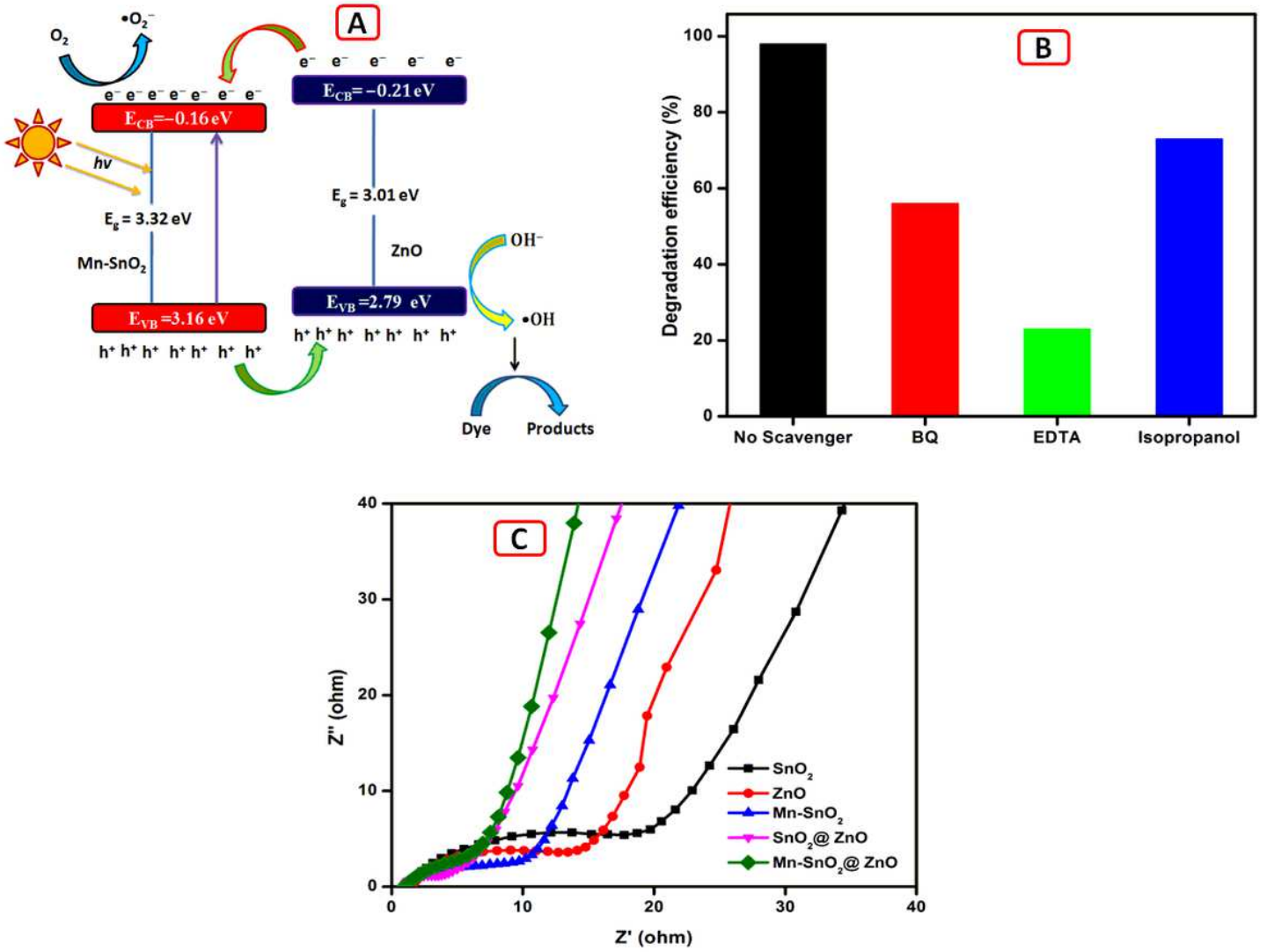

Figure 12

(A) Schematic diagram of the catalytic mechanism of Mn-SnO2@ZnO photo-catalyst, (B) Trapping experiment for the Mn-SnO2@ZnO photo-catalyst using MB dye, (C) EIS spectra of SnO2, ZnO, Mn-SnO2, SnO2@ZnO and Mn-SnO2@ZnO samples.